Accepted Preprint first posted on 28 April 2015 as Manuscript ERC-14-0546

Pituitary tumors contain a side population with tumor stem cell-associated characteristics

Freya Mertens[1], Lies Gremeaux[1], Jianghai Chen[1,2,+], Qiuli Fu[1,3], Christophe Willems[1], Heleen Roose[1], Olivier Govaere[4], Tania Roskams[4], Carolina Cristina[5], Damasia Becú-Villalobos[6], Mark Jorissen[7], Vincent Vander Poorten[8], Marie Bex[9], Johannes van Loon[10] and Hugo Vankelecom[1,++]

[1]Department of Development and Regeneration, Cluster Stem Cell Biology and Embryology, Research Unit of Stem Cell Research, KU Leuven (University of Leuven), Leuven, Belgium; [2]Department of Hand Surgery, Tongji Medical College, Union Hospital, Huazhong University of Science & Technology (HUST), Wuhan, Hubei, China; [3]Eye Center, Second Affiliated Hospital, School of Medicine, Zhejiang University, Hangzhou, and Key Laboratory of Ophthalmology of Zhejiang Province, China; [4]Department of Imaging and Pathology, KU Leuven; [5]CITNOBA (National Research Council of Argentina), National University of the Northwest of Buenos Aires (CONICET-UNNOBA), Pergamino, Buenos Aires, Argentina; [6]Lab. of Pituitary Regulation, Instituto de Biologia y Medicina Experimental, CONICET, Buenos Aires, Argentina; [7]Unit Head and Neck Oncology, [8]Research Group Experimental Oto-rhino-laryngology, [9]Unit Clinical and Experimental Endocrinology, and [10]Research Group Experimental Neurosurgery and Neuroanatomy, University Hospitals Leuven, Leuven, Belgium.

[++]Corresponding author: Hugo Vankelecom, Department of Development and Regeneration, Cluster Stem Cell Biology and Embryology, Research Unit of Stem Cell Research, KU Leuven, Campus Gasthuisberg O&N4, Herestraat 49, B-3000 Leuven, Belgium. Fax: +32-16-330642. Phone: +32-16-330692. Email address: Hugo.Vankelecom@med.kuleuven.be. [+]Co-corresponding author: Jianghai Chen, Department of Hand Surgery, Tongji Medical College, Union Hospital, Huazhong University of Science & Technology (HUST), Jiefang Avenue 1277#, Wuhan, Hubei 430022, P.R. China. Phone: +86 27 8535 1628. Email address: chenjianghai@hust.edu.cn.

Keywords: pituitary, adenoma, side population, epithelial-mesenchymal transition, tumor stem cells, cancer stem cells, stem cells, Sox2, Cxcr4.

ABSTRACT

Pituitary adenomas cause significant endocrine and mass-related morbidity. Only little is known about mechanisms underlying pituitary tumor pathogenesis. We searched for a side population (SP) in pituitary tumor, representing cells with high efflux capacity and potentially enriching for tumor stem cells (TSC). Human pituitary adenomas contain a SP irrespective of hormonal phenotype. This adenoma SP, as well as the purified SP (pSP) depleted from endothelial and immune cells, enriches for cells that express 'tumor stemness' markers and signaling pathways, including epithelial-mesenchymal transition (EMT)-linked factors. Pituitary adenomas were found to contain self-renewing sphere-forming cells, considered a property of TSC. These sphere-initiating cells were recovered in the pSP. Because benign pituitary adenomas do not grow *in vitro* and failed to expand in immunodeficient mice, the pituitary tumor cell line AtT20 was further used. We identified a SP in this cell line and found it more tumorigenic than the non-SP 'main population'. Of the two EMT-regulatory pathways tested, inhibition of C-X-C chemokine receptor type 4 (Cxcr4) signaling reduced EMT-associated cell motility *in vitro* as well as xenograft tumor growth, whereas activation of TGFβ had no effect. The adenoma pSP also showed upregulated expression of the pituitary stem cell marker *SOX2*. Pituitaries from dopamine receptor D2 knockout (*Drd2*$^{-/-}$) mice bearing prolactinomas, contain more pSP, Sox2^{+} and colony-forming cells than wildtype glands. In conclusion, we detected a SP in pituitary tumor and identified TSC-associated characteristics. Our study adds new elements to the unravelment of pituitary tumor pathogenesis and may lead to new therapeutic targets.

INTRODUCTION

Pituitary tumors are generally considered as benign adenomas. Radiology and autopsy, often performed for other-than-pituitary-related medical reasons, show a high prevalence of 10-15% in the overall population although most of these lesions are small and asymptomatic (Daly *et al.* 2009; Melmed 2011). Clinically relevant pituitary adenomas have a lower prevalence of ~0.1% (Daly *et al.* 2009), but still represent the third most frequent intracranial neoplasm after meningiomas and gliomas. Tumorigenesis in the pituitary can pose serious medical complications. Tumors may hypersecrete one or more of the pituitary hormones, leading to severe endocrine disturbances and pernicious impact on the many physiological processes governed by the gland. Growth hormone (GH)-producing adenomas (somatotropinomas, GH-A) cause gigantism or acromegaly, ACTH-producing tumors (corticotropinomas, ACTH-A) lead to Cushing's disease and prolactin (PRL)-producing adenomas (prolactinomas, PRL-A) negatively affect gonadal status and reproduction. Conversely, a large number of pituitary tumors do not measurably secrete hormones (i.e. non-functioning adenomas, NF-A), but their growth and expansion may lead to deficient function of the gland (hypopituitarism) and visual disturbances due to compression of the optic chiasm and nerves. In general, 30-45% of the clinically diagnosed adenomas display this local expansion as well as invasion of neighboring structures such as the bony sphenoid sinus and the parasellar venous cavernous sinuses (Galland *et al.* 2010). Current therapeutic approaches that include transsphenoidal resection, pharmacotherapy and irradiation remain inadequate in a significant number of patients (Daly *et al.* 2009; Galland *et al.* 2010). The degree of invasiveness appears a critical determinant for the success rate of surgical removal and thus for relapse. At present, mechanisms underlying the pathogenic processes of initiation, expansion, invasion and/or relapse of pituitary tumors are largely uncomprehended. Only a minority (~5%) of the tumors are hereditary and traced back to genetic mutations, existing either as isolated tumors or as a component of a larger endocrine syndrome like Men-1 (Daly *et al.* 2009; Melmed 2011).

In other types of tumors, so-called cancer stem cells (CSC) have been identified, a pool of relatively undifferentiated transformed cells that self-renew and propagate the entire range of tumor cell progeny. Compared to the other cells in the tumor, the CSC subpopulation is considered more tumorigenic and more resistant to therapy, thereby surviving treatment and finally re-growing the (heterogeneous) tumor (Vankelecom & Gremeaux 2010; Clevers 2011; Vankelecom 2012; Vankelecom & Chen 2014). Recently, CSC have been reported to display characteristics of epithelial-mesenchymal transition (EMT) which may drive these cells in tumor expansion and invasive activity (Mani *et al.* 2008; Morel *et al.* 2008; Kong *et al.* 2010; Pirozzi *et al.* 2011; Yoon *et al.* 2012). EMT represents a multi-step cell-conversion process during which epithelial cells gradually acquire mesenchymal features. Cells change morphology, lose polarity and cell-cell contacts (e.g. by loss of E-cadherin), become mobile with enhanced invasive capacity, and acquire increased resistance to apoptosis. More in general, EMT is known to play a key role in cancer pathogenesis, particularly during growth, maintenance (including resistance to hostile conditions) and progression of the tumor with local invasion and/or metastasis (De Craene & Berx 2013). In several types of cancer, it was discovered that EMT markers are enriched in the CSC fraction, that induction of EMT causes upregulated expression of 'stemness' genes, and that EMT acts as a key driver in the generation and activity of the CSC (Mani *et al.* 2008; Morel *et al.* 2008; Kong *et al.* 2010; Pirozzi *et al.* 2011; Yoon *et al.* 2012).

Although presence and functional (or clinical) relevance of CSC is increasingly documented in a variety of cancers (Clevers 2011; Eppert *et al.* 2011; Chen *et al.* 2012; Schepers *et al.* 2012; Boumahdi *et al.* 2014; Vanner *et al.* 2014; Zhu *et al.* 2014), the concept remains debated and is likely not applicable to all types of cancer. Nonetheless, the model may help to understand pathogenesis, therapy resistance and recurrence of tumors. At present, CSC have mostly been identified in malignant types of cancer. Whether benign tumors also contain CSC (then better referred to as tumor stem cells or TSC) has only limitedly been studied (Vankelecom & Gremeaux 2010; Lapouge *et al.* 2011; Boumahdi *et al.* 2014). The search for CSC is generally performed on the basis of 'stemness'-

102 associated membrane markers or of functional traits. High efflux capacity, mediated by ATP-binding
103 cassette (ABC) multidrug transporters, is considered one functional property of CSC, rendering the
104 cells more resistant to chemotherapeutic drugs. In the present study, we searched for cells
105 possessing such efflux capacity using the 'side population' (SP) technique (Chen *et al.* 2005, 2009).
106 Cells extruding Hoechst dye are observed as a side branch of Hoechst^{low} cells in dual-wavelength
107 FACS analysis. In a variety of cancer types, a SP has been identified and found enriched in CSC or CSC-
108 like cells (Patrawala *et al.* 2005; Wu & Alman 2008; Kato *et al.* 2010; Britton *et al.* 2012; Moti *et al.*
109 2014). Thus, we searched for SP cells in human pituitary adenomas and in additional models of
110 pituitary tumor (mouse tumor, cell line, xenograft tumors). We identified a SP and observed
111 molecular and functional characteristics supportive of a TSC-associated phenotype. In addition, we
112 identified the Cxcr4 pathway as an interesting target for further investigation in pituitary tumor
113 treatment.
114

MATERIALS AND METHODS

Pituitary adenomas

Human pituitary adenoma samples were obtained immediately after transsphenoidal resection at the University Hospitals Leuven (Division Neurosurgery). Informed consent was received from the patients. Hormonal phenotype was determined by the Department of Imaging and Pathology (University Hospitals Leuven). An overview of the samples with clinical data is provided in Table 1. Genders are represented equally with an average age of 53 yr (range: 19-84 yr) at the time of surgery. The majority of the tumors are NF-A (n=34) and GH-A (n=21). Other types of resected pituitary tumors typically are microadenomas only yielding sufficient study material in a limited number of cases (ACTH-A; n=3), or are not surgically removed but treated pharmacologically (resected PRL-A; n=2).

Tumor samples were either immediately processed for flow-cytometric analysis after resection, or cryopreserved as small pieces in Leibovitz-L-15 medium (Life Technologies, Carlsbad, CA) supplemented with 10% fetal bovine serum (FBS; Lonza, Rockland, ME) and 10% dimethylsulfoxide (DMSO; Sigma-Aldrich, Bornem, Belgium) followed by storage at -196°C for later examination. The freezing procedure did not change the SP proportion (see Supplementary Fig. S1) or the expression characteristics as evident from the microarray analyses.

Dissociation of human pituitary adenoma into single cells

Tumor samples were rinsed in Dulbecco's Modified Eagle's Medium (DMEM; Life Technologies) supplemented with 0.3% bovine serum albumin (BSA; Serva, Heidelberg, Germany) and incubated with collagenase type IV (1mg/ml in Medium 199; Life Technologies) for 2-2.5 hr at 37°C. Cell debris was removed by centrifugation through a 3% BSA layer. The resultant cell pellet was resuspended in pituitary-optimized, serum-free chemically defined medium (SFDM, Life Technologies; supplemented with 0.5% BSA; Chen *et al.* 2005, 2009) for further analyses.

Immunohistology of human pituitary adenoma sections

Formalin-fixed paraffin-embedded pituitary adenoma blocks were obtained from the Biobank (University Hospitals Leuven). Antigen retrieval was performed on 5-µm sections using EnVision FLEX Target Retrieval Solution (Dako, Glostrup, Denmark). Endogenous peroxidase activity was blocked using EnVision Peroxidase-Blocking Reagent and sections were incubated with primary antibodies directed against human E-cadherin (Ready-to-use; Dako), vimentin (1/500; Dako), NOTCH2 (1/200; Abcam, Cambridge, UK) and IL-6 (1/200; Abcam). Subsequently, samples were processed using EnVision Dual Link (Dako). The complex formed was visualized with 3,3'-diaminobenzidine (DAB; Dako) and sections were counterstained with hematoxylin (Dako).

Isolation and dissociation of mouse pituitary

C57/Bl6 mice were purchased from Elevage Janvier (BioServices, Uden, The Netherlands), and dopamine D2 receptor knockout (*Drd2*$^{-/-}$) mice from The Jackson Laboratory (Bar Harbor, ME). Mice were kept or bred in the KU Leuven Animal Facility under conditions of constant temperature, humidity and day-night cycle in a sterile environment. Food and water were supplied *ad libitum*. Animal experiments were approved by the KU Leuven Ethical Committee.

The pituitary was isolated from euthanized mice as previously described (Chen *et al.* 2005, 2009). The anterior lobe (anterior pituitary, AP) of the *Drd2*$^{-/-}$ mice growing prolactinomas (from 6 to 14 months of age; Cristina *et al.* 2006), and of the respective control mice (*Drd2*$^{+/-}$ and *Drd2*$^{+/+}$) was dispersed into single cells using collagenase type IV as explained above for human pituitary adenomas.

Culture and treatment of AtT20

The mouse corticotrope AtT20 cell line was obtained from American Type Culture Collection (ATCC, CCL-89; Manassas, VA). The cell line was authenticated by hormone expression analysis with RT-quantitative (q)PCR (see below). The cells were cultured in DMEM/F12 (Life Technologies)

supplemented with 10% FBS. To investigate involvement of the transforming growth factor-β (TGFβ) or Cxcr4 pathways, AtT20 cells were cultured in serum-free medium for 18-24 hr and then treated with TGFβ1 (5ng/ml; R&D Systems, Minneapolis, MN) or AMD3100 (octahydrochloride, 100ng/ml; Sigma-Aldrich), respectively. Medium was refreshed every 24 hr. To analyze gene expression and SP proportion after treatment (see below), cells were detached and dissociated using trypsin (0.05%) with EDTA (0.02%; Life Technologies).

Flow cytometry

Dissociated cells (from human adenoma or mouse AP, AtT20 cell line or xenograft tumors – see below) were processed for SP analysis as described in detail before (Chen *et al.* 2005, 2009). In short, cells were incubated with the vital dye Hoechst33342 (Sigma-Aldrich) at a final concentration of 2.5µg/ml (for mouse AP and AtT20) or 5µg/ml (for adenoma and xenograft samples). Subsequently, cells were either immediately analyzed by FACS (Vantage or Aria III; BD Biosciences) or first stained with phycoerythrin (PE)-conjugated mouse anti-human CD45, FITC-conjugated mouse anti-human CD31, PE-conjugated mouse anti-mouse CD45 and/or FITC-conjugated rat anti-mouse CD31 antibodies, using dilutions recommended by the manufacturer (BD Biosciences). Samples were examined for SP on the basis of dual-wavelength emission using appropriate filters (Vantage: 424/44 and 630/22; Aria III: 450/40 and 630/20) after (near-)UV excitation (360 and 375nm on Vantage and Aria III, respectively). The SP phenotype was verified by adding verapamil (100µM; Sigma-Aldrich) which blocks the Hoechst efflux. The bulk cell population not expelling Hoechst is designated as the 'main population' (MP). CD31 and CD45 staining was controlled using isotype antibodies (BD Biosciences; data not shown).

Xenograft tumors and *in vivo* tumorigenic activity

In an attempt to grow human pituitary adenoma in immunodeficient mice, tumor pieces or dissociated cells (1-1.5x10^6) were transplanted subcutaneously (sc) (GH-A and NF-A, n=8) or under

the kidney capsule (GH-A and ACTH-A, n=3). Male mice (6-10 weeks old) with increasing grade of immunodeficiency (from SCID, NOD-SCID to NOD-SCID$^{IL2Rγ-/-}$) were purchased from Elevage Janvier, and were anesthetized with Avertin (tribromoethanol; Sigma-Aldrich). Prior to injection, cells were resuspended in DMEM mixed with Matrigel (1:1; BD Biosciences). Three to six months later, mice were examined for tumor growth after euthanasia. Tissue of implantation sites was dissected and hematoxylin/eosin (H&E) staining performed.

To grow xenograft tumors from AtT20 cells, SCID mice (male; 6-10 weeks old) were sc injected with $5x10^5$ cells. To assess tumorigenic (TSC) activity of the AtT20 SP *versus* the MP, cell populations were sorted into DMEM/F12/10% FBS, mixed with Matrigel (1:1), and sc injected at different cell numbers into SCID mice (SP cells in one flank, the similar number of MP cells in the other flank of the same mouse). Tumor size was measured using a caliper and volume calculated with the formula '[(large side) x (small side)^2] x 0.52'.

To explore the involvement of the Cxcr4 pathway, AtT20 xenograft tumors developing in SCID mice were treated with AMD3100 by intratumoral injection (5µg, two times/week), starting from day 21 after sc AtT20 cell implantation.

Tumorsphere- and colony-forming assay

Dissociated human pituitary adenoma cells were seeded at a density of 100 000 cells/ml in 35-mm non-treated culture dishes (Iwaki, Scitech, Chiba, Japan) and cultured in SFDM, supplemented with B27 (1:50; Life Technologies) and recombinant basic fibroblast growth factor (bFGF, 20ng/ml; R&D Systems). Fresh medium was added every 3 days. To assess self-renewal capacity, spheres were harvested, dissociated into single cells using trypsin (Chen *et al.* 2009) and cells re-seeded under similar conditions.

To evaluate colony-forming capacity, cells were cultured at low density (1000-4000 cells/60-mm dish) in Ultraculture medium (Life Technologies) to which 5% FBS, 20ng/ml bFGF and 50ng/ml cholera toxin (Sigma-Aldrich) were added. Medium was changed every 3 days. Cultures were fixed

with methanol and stained with 1,9-dimethyl-methylene blue (Sigma-Aldrich), and the number of colonies was determined. Live pictures of the formed spheres and colonies were taken using a Nikon Eclipse TS100 microscope (Nikon Instruments, Melville, NY).

Cell motility assay

Cell motility was evaluated using the 'scratch assay'. After reaching 90% of confluence, AtT20 cells were serum-starved for 24 hr and then treated with mitomycin C (10µg/ml; Kyowa, Tokyo, Japan) to inhibit cell proliferation. A straight scratch was created and cells were further kept in DMEM/F12, together with TGFβ1 (5ng/ml), AMD3100 (100ng/ml) or vehicle. Medium was changed every 24 hr. Migration of cells into the scratch was evaluated by light microscopy and live pictures were taken with the Nikon Eclipse TS100 microscope at different time points. The open area was calculated using analysis algorithm-based T-scratch software (CSElab–ETH, Zürich, Switzerland).

Small-animal magnetic resonance imaging

Magnetic resonance imaging (MRI) was performed on *Drd2*$^{-/-}$ and *Drd2*$^{+/-}$ mice using a horizontal 9.4-Tesla nuclear magnetic resonance spectrometer and a 40-mm-diameter birdcage coil as radio frequency transmitter and receiver. Mice were anesthetized using 1% isoflurane in a mixture of 75% air and 25% oxygen. T1-weighted images were acquired using a two-dimensional multiple-slice spin echo sequence, with an echo time of 11 msec, a repetition time of 500 msec, in-plane resolution of 0.1x0.1 mm, 24 coronal slices with 0.3-mm slice thickness, and 10 signal averages. Image reconstruction was performed using the spectrometer console. Ten minutes prior to the scanning procedure, mice received an intraperitoneal injection of the contrast agent gadolinium (0.50mmol/kg body weight).

Immunofluorescence analysis

For immunofluorescence examination of mouse pituitaries, whole glands were isolated and fixed with paraformaldehyde (4%; Riedel-de Haën, Seelze, Germany). After agarose embedding, pituitaries were coronally sectioned to 45-µm slices using a vibratome (Microm HM 650V; Prosan, Merelbeke, Belgium). Sections were permeabilized with 0.4% Triton-X 100 (Sigma-Aldrich) and incubated overnight with the following primary antibodies: goat anti-human SOX2 (1/750; Immune Systems, Devon, UK) and rabbit anti-mouse prolactin (PRL) (1/10 000; from Dr. A.F Parlow, NHPP, Harbor-UCLA Medical Center, Torrance, CA). Finally, sections were incubated with AlexaFluor 488-conjugated donkey anti-rabbit and/or AlexaFluor 555-conjugated donkey anti-goat antibodies (1/1000; Life Technologies), and nuclei labeled with ToPro3 (Life Technologies). Immunofluorescence was examined using a Zeiss LSM 510 confocal laser-scanning microscope (Zeiss, Zaventem, Belgium) accessible through the Cell Imaging Core (CIC; KU Leuven). Z-stacks were collected and analyzed using Zeiss LSM Image Browser and ImageJ (http://imagej.nih.gov/ij/), and pictures were prepared using the same programs and Microsoft PowerPoint (2007).

Immunofluorescence staining of paraffin-embedded mouse pituitary sections (5µm) was performed after antigen retrieval with citrate buffer (pH 6) and permeabilization with Triton-X 100 (0.1% in PBS). Following incubation with primary and secondary antibodies (as above), sections were covered with Vectashield (containing 4',6-diamidino-2-phenylindole or DAPI) and analyzed using a Leica DM5500 epifluorescence microscope (Leica Microsystems, Diegem, Belgium) accessible through InfraMouse (KU Leuven-VIB). Recorded images were converted to pictures with ImageJ and Microsoft PowerPoint (2007).

Cytospin samples of dissociated mouse AP cells were fixed with paraformaldehyde (4%), permeabilized with saponin (0.5%; Sigma-Aldrich), and further immunostained for Sox2 (with goat anti-human SOX2 at 1/250; Immune Systems) as described above. In some analyses, cells were at the same time immunostained for the proliferation marker Ki67 (with rabbit anti-Ki67 at 1/50; Thermo Scientific, Fremonet, CA). Nuclei were counterstained with DAPI (0.5µg/ml). To enumerate Sox2-

immunopositive cells, pictures were captured using the Leica DM5500 microscope, and cells counted with ImageJ in 5 to 10 random fields per group in each experiment (about 1500 cells per group in each experiment). The proportions of the $Sox2^+$ cells (on total cells counted) were determined. Because of the increase of total AP cells in the *Drd2*$^{-/-}$ adenomatous pituitary, comparison of proportions is not appropriate. Thus, absolute numbers of $Sox2^+$ cells were calculated (using their proportion and the total number of AP cells obtained per experimental group of mice) for comparison between *Drd2*$^{-/-}$, *Drd2*$^{+/-}$ and *Drd2*$^{+/+}$ mice.

For immunofluorescence examination of tumorspheres developed from human pituitary adenomas, fixation with paraformaldehyde (4%) and permeabilisation with Triton-X100 (0.4% in PBS) were followed by incubation with goat anti-human SOX2 (1/250; Immune Systems), rat anti-mouse nestin (1/500; Abcam) and/or rabbit anti-human GH (for spheres originating from GH-A; 1/2000; Dako). Secondary antibodies included AlexaFluor 555-conjugated donkey anti-goat, AlexaFluor 488-conjugated donkey anti-rat, and AlexaFluor 488-conjugated donkey anti-rabbit (all at 1/1000; Life Technologies). Pictures were obtained with the Leica DM5500 epifluorescence microscope as described above.

AtT20 cell death, apoptosis and proliferation

The number of dying or dead AtT20 cells after AMD3100 treatment (100ng/ml) was determined after staining with Trypan Blue (0.4%; Sigma-Aldrich). Apoptosis was scored by TUNEL (Terminal deoxynucleotidyl transferase dUTP nick end labeling) analysis in cytospin samples of AtT20 cells from culture or xenograft tumors, using the FragEL kit (Calbiochem, Darmstadt, Germany). Cell proliferation was quantified by immunofluorescence staining of cytospin samples for Ki67 as described above. Pictures were taken and cells enumerated (see above).

Whole-genome expression profiling

Total SP and MP cells (NF-A, n=5; GH-A, n=4) or $CD31^-/CD45^-$ SP (purified SP or pSP) and pMP cells (NF-A, n=5) were sorted by FACS into cold lysis solution of the RNeasy Micro Kit (Qiagen, Venlo, The Netherlands). Total RNA was extracted immediately after cell collection according to the manufacturer's guidelines. RNA samples were stored at -80°C until further processing for whole-genome expression profiling (in collaboration with the VIB Nucleomics Core, KU Leuven). RNA quality and concentration were determined using Agilent Picochips on an Agilent BioAnalyzer 2100 (Agilent Technologies, Santa Clara, CA). Two ng of high-quality RNA (with RNA Integrity Number ≥8.0) was amplified using the NuGen Pico WTA kit (NuGen Technologies, San Carlos, CA). Cy3 label was incorporated into the cRNA probes which were then hybridized onto Agilent whole human genome 44K oligonucleotide arrays. Slides were scanned and data processed using the Agilent's Feature Extraction Software for background correction, quantile normalization, Principal Component Analysis (PCA), hierarchical clustering, and MA and Volcano plots. Microarray data are available from the NCBI's Gene Expression Omnibus (GEO, http://www.ncbi.nlm.nih.gov/projects/geo/) through series accession number GSE62960.

To determine differentially expressed genes (probes), a stringent analysis was initially applied to the normalized data sets. Taken into account that the data are paired (SP *versus* MP for each sample), analysis was based on the $\log_2$-ratios computed for each pair. Log_2-ratios were compared with the Limma (Linear Models for Microarray Data) package of Bioconductor in R and a moderated t-statistic (implemented in Limma) was performed to test the significance of the obtained differences. For the first microarray data set (total SP *versus* MP), the resulting p-values were corrected for multiple testing with Benjamini-Hochberg to control the false discovery rate. Differentially expressed genes were withheld when the corrected p-value was lower than 0.05. For the second microarray data set ($CD31^-/CD45^-$ SP *versus* $CD31^-/CD45^-$ MP), Benjamin-Hochberg could not be applied because of the low number of samples. Therefore, a cut-off based on the uncorrected p-values ($p<0.001$) was utilized. For both data sets, the cut-off on the p-values was

combined with a cut-off on the fold change (≥2) to finally determine the differentially expressed genes.

Given the not yet large number of adenomas analyzed, causing a very high cut-off for differential expression and hence the discard of potentially interesting differences, we additionally applied a less stringent analysis by paired Students t-test performed on the individual probe sets. Genes were judged differentially expressed when $p<0.05$ and fold change ≥1.5. We further considered genes that showed a significant expression difference in not all but in 5 to 8 out of the 9 adenomas analyzed for total SP and MP, and in 2 to 4 out of the 5 adenomas examined for $CD31^-/CD45^-$ fractions.

Functional clustering analysis of differentially expressed genes (Gene Ontology, GO) was performed using the Database for Annotation, Visualization and Integrated Discovery (DAVID, version 6.7; www.david.abcc.ncifcrf.gov). Gene clusters with enrichment score >1.5 (-log of the median p-value for the functional group) were retained. Finally, we narrowed the gene sets by focusing on factors shown to be important in CSC/'tumor stemness' including EMT, NOTCH, WNT/β-CATENIN and TGFβ/BMP.

Gene expression analysis by RT-qPCR

Amplified cDNA of the $CD31^-/CD45^-$ SP and MP fractions from the 5 microarrayed NF-A samples, as well as from 2 additional samples (NF-A, n=1; GH-A, n=1; see Table 1), was examined by RT-qPCR to validate expression of a selection of genes using Fast SYBR Green Master Mix on an ABI 7900HT Fast RT-PCR system, performed according to the manufacturer's instructions (Life Technologies).

Gene expression analysis of AtT20 cells or dispersed xenograft tumors occurred using a similar approach (but without the RNA amplification step). cDNA was subjected to qPCR in a LightCycler 480 using the LightCycler FastStart DNA Master Plus SYBR Green I (Roche, Basel, Switzerland).

Forward and reverse primers were designed using PerLPrimer (http://perlprimer.sourceforge.net) or obtained from a public database

(http://medgen.ugent.be/rtprimerdb), and are described in Supplementary Table S1. Glyceraldehyde-3-phosphate dehydrogenase (GAPDH), β2-microglobulin (B2M) and/or hypoxanthine phosphoribosyltransferase 1 (HPRT1) were used to normalize gene expression. Their expression was found to be stable (data not shown). Relative gene expression levels were calculated as ΔCt values ('Ct target minus Ct reference') and compared between the SP and MP as fold change ($2^{-\Delta Ct}$ SP/$2^{-\Delta Ct}$ MP). Statistical analysis was performed using Graphpad Prism (Version 5.2; Graphpad Software, La Jolla, CA) applying the Mann-Whitney U test. P-values <0.05 were considered as statistically significant.

For authentication of the AtT20 cell line used, hormone gene expression was examined by RT-qPCR. The corticotrope phenotype of the cell line was confirmed by detection of *pro-opiomelanocortin* (*POMC*; precursor of ACTH) expression, while *GH* and *thyroid-stimulating hormone-β* (*TSHβ*) gene transcription was not found (see Supplementary Table S2).

359 ## RESULTS

360 **Human pituitary tumors contain a side population**

361 Human pituitary adenomas (n=60; see Table 1) were examined for the presence of a SP. In all
362 tumors analyzed, a Hoechst^{low} cell population was detected which was not observed anymore when
363 the efflux-blocker verapamil was added together with Hoechst (Fig. 1A), thereby demonstrating the
364 SP phenotype (mean SP ± SEM: 1.9% ± 0.3 of the total viable tumor cells; range: 0.4-17.2%; Table 1).
365 SP proportions were not different between the samples analyzed immediately after surgical
366 resection (n=24) or after cryopreservation (n=36) (Table 1; Supplementary Fig. S1A), neither between
367 the different hormonal phenotypes examined (Fig. 1B; Table 1). The adenoma SP predominantly
368 clusters cells of small to medium size (low 'forward scatter') and low granularity (low 'side scatter')
369 (Supplementary Fig. S1B).

370

371 **Whole-genome expression profiling of the adenoma SP points to epithelial-mesenchymal**
372 **transition and 'tumor stemness'**

373 SP cells and the tumor bulk MP cells from somatotropinomas (GH-A, n=4) and non-functioning
374 adenomas (NF-A, n=5; see Table 1) were sorted by FACS and subjected to gene expression profiling
375 using whole-genome microarrays. Principal component analysis (PCA) indicates a comparable
376 segregation of the SPs from the corresponding MPs for the majority of the samples analyzed
377 (Supplementary Fig. S1C). Hierarchical clustering of differentially expressed genes also largely
378 separates the SPs from the MPs (Supplementary Fig. S1D).

379 The set of genes most differentially expressed ($p<0.001$; 2760 probe sets) was submitted to
380 DAVID for Gene Ontology (GO) analysis, yielding a total of 1688 corresponding human ENSEMBL IDs.
381 Gene set enrichment exposes in the SP upregulation of biological functions involved in cell
382 proliferation, vascular development, cell migration and motility, and lymphocyte activation
383 (Supplementary Table S3).

A focused analysis of a selection of genes using the expression data of the 9 adenomas (Table 2 and Supplementary Table S4) reveals upregulated expression (i.e. >1.5-fold in at least 2/3rd, or in 5 of the 9 tumors, $p<0.05$; see Materials and Methods) in the SP of the multidrug transporters *ABCB1* and *ABCG2* that typically underlie the SP phenotype, thereby validating the SP identification and sorting procedure. Remarkably, the transcriptome displays an expression pattern that supports occurrence of EMT in the SP compartment. The epithelial markers E-cadherin (*CDH1*) and claudin-1 (*CLDN1*) are downregulated in the pituitary adenoma SP whereas the mesenchymal markers vimentin (*VIM*) and fibronectin (*FN1*) are upregulated (Table 2 and Supplementary Table S4). Moreover, recognized markers of EMT such as *SNAI1, ZEB1* and *ZEB2* (all transcriptional repressors of the *CDH1* gene) are higher expressed in the SP *versus* the MP together with other inductors and regulators of EMT (*KLF8, LEF1, TCF4, FOXC1, HOXB9, FOSL2, MMP1/2* and *CXCR4*). Some of the pathways identified as upregulated are also well known for their regulatory input in EMT (WNT, TGFβ, epiregulin or ERG, amphiregulin or AREG). In this analysis, we also observed that factors often associated with 'tumor stemness' or CSC, including *CD44, CXCR4, KIT, KLF4* and *NESTIN* are upregulated in the SP. In addition, the signaling pathways of NOTCH, WNT and TGFβ□BMP have also been related to 'tumor stemness'. Overall, no obvious differences were observed between the SP transcriptomes of the NF-A and the GH-A samples.

Of note, the microarray analysis also revealed upregulated expression of genes associated with an endothelial phenotype (such as *PECAM1/CD31, VWF, CDH5, VCAM1, FLK1/KDR, TIE1, TEK/TIE2*) or an immune character (such as *CD45/PTPRC*) in the adenoma SP (see Table 2 and Supplementary Table S4). These expression characteristics are in line with the enriched biological processes as described above (*viz.* vascular development and lymphocyte activation; see Supplementary Table S3) and suggest the presence of endothelial and immune/hematopoietic cells in the SP. Before, we and others have discovered that the SP, whether from healthy tissue or tumors, represents a still heterogeneous population, not only segregating cells with (tumor) stem cell properties but also some

other cells of endothelial and immune/hematopoietic phenotype (Chen *et al.* 2009; Pfister *et al.* 2005; Uezumi *et al.* 2006).

Taken together, our microarray expression data indicate that, compared with the MP, the pituitary adenoma SP is enriched in cells with EMT- and 'tumor stemness'-associated molecular traits, but is still heterogeneous in cell phenotypes.

EMT- and 'tumor stemness'-related expression characteristics remain present in the adenoma SP depleted from endothelial and immune cells

The pituitary adenoma SP was then analyzed for the presence of endothelial ($CD31^+$) and immune/hematopoietic ($CD45^+$) cells. Flow cytometry revealed a $CD31^+$ cell population of varying abundance in the SP (mean ± SEM: 50.9 ± 4.8% of the SP; range: 5.8–95.2%; n=37; Fig. 1C-D and Table 1). Also $CD45^+$ cells are found but in general constitute a lower fraction of the adenoma SP (16.2 ± 3.0% of the SP; range: 0.2-66.6%; n=31; Fig. 1C-D and Table 1). The non-endothelial, non-immune ($CD31^-/CD45^-$) SP fraction finally comprises on average $1/3^{rd}$ of the total SP (32.3% ± 2.2; range: 7.2 – 64.1%), 0.5% (± 0.1) of all $CD31^-/CD45^-$ adenoma cells and 0.1% (± 0.01) of the total tumor cell population. In general, no correlation was found between the size of the total SP and the proportion of $CD31^+$ or $CD45^+$ cells (Table 1 and Fig. 1D), although the 2 samples with the highest SP proportion analyzed for these antigens (PA 26, PA 43) contain the largest fraction of $CD31^+$ cells in the SP.

To determine whole-genome expression profiles of the non-endothelial, non-immune cell populations, SP and MP were depleted from $CD31^+/CD45^+$ cells during flow-cytometric sorting (see Fig. 1C for gating; n=5 NF-A; Table 1). Stringent analysis revealed 101 genes (probe sets), corresponding to 74 human ENSEMBL IDs in DAVID, which are differentially expressed between the $CD31^-/CD45^-$ SP (further referred to as the purified SP or pSP) and the $CD31^-/CD45^-$ MP (pMP), 80 of which are upregulated in the pSP and 21 downregulated (see Supplementary Fig. S2A-C). The as yet relatively small number of samples analyzed causes a high cut-off for differential expression (as is

clear from Supplementary Fig. S2A). Therefore, we performed an additional, less stringent examination (see Materials and Methods), analyzing genes not only altered (≥ 1.5-fold, $p<0.05$) in all adenomas, but also in 4 out of the 5 tumors profiled. A total of 2374 genes (probe sets) were found to be differentially expressed in the pSP compared to the pMP in at least 4 of the adenoma samples (corresponding to 1576 human ENSEMBL IDs), with 1662 and 712 genes up- and downregulated, respectively (Supplementary Table S5). The gene sets obtained in both the stringent and less stringent analyses (101 and 2374 genes, respectively) were submitted to GO examination using DAVID. Overviews of the most significantly enriched biological processes are provided in Supplementary Table S6 and S7, and include, amongst others, cell motility and migration, vascular development, cell proliferation and organ development.

Subsequent analysis of the pSP was focused on a selection of genes as considered above for the total SP, including genes associated with EMT and 'tumor stemness' (Table 3 and Supplementary Table S8). On the whole, the expression picture of the total SP appears retrieved in the $CD31^-/CD45^-$ SP, *viz.* upregulated expression of *ABCG2* and of other CSC-associated markers including *CD44*, *CD34*, *LIFR* and *CXCR4*. *KIT* expression is upregulated in 4 of the 5 samples and *NESTIN* in 3 of the 5 (Table 3). In particular, the gene expression picture underlying EMT is also present in the pSP, showing elevated expression of the mesenchymal markers *VIM* and *FN1* and of several transcriptional EMT regulators (including *SNAI1*, *SNAI2*, *ZEB1, ZEB2*) (Table 3). Since GO enrichment pointed to gene clusters involved in cell motility and migration, and EMT is known to drive motile and invasive behavior of cells, additional genes involved in these processes were examined. A considerable number were found to be up- or downregulated in the pSP *versus* the pMP including *EPHB1* and *TM4SF1* (Supplementary Table S8). Interestingly, also epidermal growth factor receptor (*EGFR*) is highly (9-fold) upregulated in the pSP (Supplementary Table S8); EGFR has been found to be involved in tumor cell migration in craniopharyngiomas (Hölsken *et al.* 2011). In addition, several components functioning in NOTCH, WNT and TGFβ signaling are elevated (Table 3 and Supplementary Table S8). These pathways play a role in EMT and 'tumor stemness' but also in pituitary development (Zhu *et al.*

2007; Vankelecom 2010). More in general, gene clusters associated with organ development and differentiation processes are found enriched in the pSP (see Supplementary Tables S4 and S5). Finally, also genes implicated in angiogenesis are upregulated in the pSP *versus* pMP (Table 3; Supplementary Tables S6, S7 and S8).

Differential expression as concluded from the pSP microarray interrogations was verified by RT-qPCR for a number of the most interesting genes (Fig. 1E). For this analysis, the 5 micro-arrayed NF-A samples were complemented with 2 additional tumors (1 NF-A and 1 GH-A; see Table 1). RT-qPCR was found to essentially confirm the microarray data, although statistical significance was not always reached in the as yet relatively limited number of samples analyzed. All 17 genes examined show upregulated expression in the pSP when compared to the pMP (9 with statistical significance, 8 with upward trend; Fig. 1E). Most remarkable are the elevated expression levels of *CD44*, *IL-6*, *NOTCH2*, *PDGFRB, SNAI2*, *VIM* and *ZEB2*, in the pSP over the pMP (>55-fold). A higher expression level (>55-fold) was also found for *CXCR4*, *FN1*, *HES1*, *PDGFC* and *TGFBR2*, not in all but in at least 5 out of the 7 samples. Expression of *CDH1* was also checked but was not significantly different in the pSP *versus* the pMP, although a trend of downregulation was measured in the pSP of 4 out of the 7 adenomas analyzed. Expression of E-cadherin, vimentin, IL-6 and NOTCH2 was further analyzed by immunohistochemistry in paraffin-embedded sections of pituitary adenomas used above for gene expression analysis (n=6; see Table 1 and Supplementary Fig. S2D). Tumors with high E-cadherin immunoreactivity contain some zones and cell clusters where E-cadherin is downregulated, and vimentin is expressed in some regions or small nests of tumor cells (in addition to the pericapillar cells), suggesting that some tumor cells may have undergone EMT. IL-6 immunoreactivity was observed in a couple of clustered cells (2-4 per section) in 3 out of the 6 adenomas analyzed, and NOTCH2 immunoreactivity in 1-2 cells per section in 4 out of the 6 adenomas (Table 1 and Supplementary Fig. S2D). IL-6 and NOTCH2 immunoreactivity were found in the same adenomas, except for PA 34.

Human pituitary tumors contain sphere-forming cells segregating to the pSP

TSC generate spheres ('tumorspheres') when brought in appropriate suspension-culture conditions (Vankelecom & Gremeaux 2010; Clevers 2011). When pituitary adenoma cells were cultured in the presence of B27 and bFGF, free-floating spheres developed progressively. After 7 days of culture bright and mostly smooth-edged spheres were obtained which clearly differ from the irregular clumps of aggregated cells that also formed (Fig. 2A-B; n=13 encompassing NF-A and GH-A). Sphere cells were found to express the stemness markers Sox2 and nestin (Chen *et al.* 2009), thereby supporting their TSC character (Fig. 2C and Supplementary Fig. S3A-B; n=3: 1 NF-A and 2 GH-A). At the end of the culture period (day 7-10), some spheres contained cells expressing the hormone produced by the original tumor, suggesting some degree of spontaneous differentiation and further supporting their TSC phenotype (Supplementary Fig. S3C). To examine the self-renewal capacity of the sphere-initiating cells (as a further property of TSC), primary spheres were dissociated and cells seeded again. Secondary spheres with similar morphology developed although fewer in number (Fig. 2D-E; n=9), likely due to a considerable loss of cells after dispersion of the primary spheres. Third-generation spheres were further also obtained, but were still scarcer (Fig. 2F).

To investigate whether the sphere-forming cells belong to the pituitary tumor's SP, $CD31^-/CD45^-$ SP cells were sorted from adenomas and seeded in sphere-forming conditions (n=3). Spheres developed in the pSP cultures (Fig. 2G) and were absent from pMP cultures that only contained irregular clumps of cells (Fig. 2G, inset). However, only very few spheres could be obtained (2-4 spheres per 20 000 pSP cells originally seeded), which made it impossible to get enough viable cells for further passaging after dispersion.

Together, our findings provide supportive evidence that human pituitary adenomas contain self-renewing sphere-forming cells that give rise to spheres expressing stemness markers, considered as properties of TSC, and further show that the sphere-initiating cells segregate to the pSP.

In addition to the *in vitro* sphere-forming assay, CSC/TSC activity is typically tested *in vivo* by (xeno-)transplantation in immunodeficient mice (Vankelecom & Gremeaux 2010; Clevers 2011; Chen

513 *et al.* 2012; Schepers *et al.* 2012; Boumahdi *et al.* 2014). However, we observed that human pituitary
514 adenoma, irrespective of hormonal phenotype, does not grow (i.e. expand) in immunodeficient SCID
515 mice. Although small tumor pieces survived for 3-4 months after sc implantation, no enlargement
516 was detected (data not shown). Xenograft adenoma growth did not only fail in SCID mice but also in
517 the more immunodeficient NOD-SCID and NOD/SCID$^{IL2R\gamma-/-}$ models, after sc implantation of tumor
518 parts as well as of dissociated cells (data not shown). Similarly, pituitary adenoma fragments
519 engrafted under the kidney capsule survived but did not visibly grow in size (as analyzed after 3-6
520 months; Supplementary Fig. S4). Therefore, to be able to further functionally characterize the
521 pituitary tumor SP and to explore its TSC-associated phenotype, we turned to a well-established
522 pituitary tumor cell line, the mouse corticotrope AtT20, previously shown to grow tumors after sc
523 implantation in immunodeficient mice (Taguchi *et al.* 2006).
524
525 **Characterization of AtT20's SP and tumorigenic activity**
526 First, we examined whether the AtT20 cell line contains a SP. A verapamil-blockable Hoechst^{low}
527 cell population was detected, amounting to 1.0% ± 0.3 of total cells (n=12; Fig. 3A). This AtT20 SP
528 shows upregulated expression of the analyzed 'tumor stemness' genes *Cd44* and *Cxcr4* (Fig. 3B).
529 To study *in vivo* tumorigenic activity, we first verified the tumor-growing capacity of AtT20 cells
530 in SCID mice. Sc injection of $5x10^5$ cells results in a gradually developing tumor (Supplementary Fig.
531 S5A), palpable after 15-20 days and further expanding in volume until the mouse becomes moribund,
532 most likely due to corticoid overproduction because of enhanced adrenal stimulation by the AtT20-
533 produced ACTH (Taguchi *et al.* 2006). A SP remains present in the AtT20-derived xenograft tumors
534 (as analyzed after 50-55 days), although the proportion is lower than in the cell line in culture (0.5%
535 *versus* 1%; n=3).
536 SP and MP cells were then sorted by FACS from cultured AtT20 cells, and varying numbers
537 (10 000, 5000 and 1000 cells) sc injected into SCID mice. Although all cell populations induced tumor
538 growth, SP-derived tumors expanded faster (Supplementary Fig. S5B) and/or became larger (Fig. 3C

and Supplementary Fig. S5B) when compared to MP-derived tumors. The SP cells developed a tumor with reconstitution of the SP/MP profile (0.5% SP; n=2) whereas the MP cells generated tumors with a lower SP portion (0.2%; n=2). Together, our results provide indications that the AtT20 SP has tumor-proliferative dominance, and that TSC(-like cells) are enriched, although not exclusively segregated, in the SP.

Effects of EMT-regulatory pathways in the AtT20 cell line

As described above, the transcriptomic data of the human pituitary adenomas support the presence of an EMT process in the (p)SP. Therefore, we tested the impact of two important EMT-regulatory pathways (De Craene & Berx 2013), i.e. of TGFβ and Cxcr4, in the AtT20 cell line. Moreover, Cxcr4 has been identified as a marker of CSC(-like cells) in various types of cancer (Hermann *et al.* 2007; Vankelecom & Gremeaux 2010; Clevers 2011). As mentioned above, its expression is upregulated in the human pituitary adenoma pSP and the AtT20 SP (Table 3, Fig. 1E and Fig. 3B). Of note, these studies could not be performed with primary human pituitary adenoma cells since these cells cannot efficiently be kept in culture and do not grow (well) *in vitro* (Hofland & Lamberts 2002).

Treatment of AtT20 cells with TGFβ1 for 72 hr significantly stimulated the expression of EMT factors *Snai2* and *Vim*, while there was a clear upward trend for *Snai1* and *Cxcr4* (Fig. 4A). However, TGFβ1 treatment did not significantly enhance the motility of AtT20 cells, which is an expected functional consequence of EMT (Fig. 4B). Treatment of AtT20 cells in culture with TGFβ1 did not significantly increase the SP proportion (1.2% ± 0.1 *versus* 1.0% ± 0.3 in control culture; n=3; $p>0.05$). Along the same line, pretreatment of AtT20 cells with TGFβ1 did not lead to a higher tumor-growing capacity when sc transplanted in SCID mice, neither regarding onset, nor regarding progression (volume expansion) of the tumor (Supplementary Fig. S5C).

563 To analyze the involvement of the Cxcr4 pathway, we treated developing AtT20 xenograft
564 tumors in SCID mice with the Cxcr4 antagonist AMD3100. Interestingly, tumors injected with
565 AMD3100 grew at a slower rate and remained smaller than vehicle-injected tumors (Fig. 4C).
566 We further observed that AMD3100 significantly reduced the migratory activity of AtT20 cells as
567 analyzed *in vitro* (Fig. 4B), thus suggesting an impact on EMT. However, AMD3100 treatment did not
568 significantly affect the expression level of the EMT-associated genes *Zeb2*, *Snai1*, *Snai2* (although a
569 downward trend was observed), *Vim* and *Cdh1*, and of the CSC-associated marker *Cd44*, as analyzed
570 in the xenograft tumors after 20 days of treatment (Fig. 4D). *In vitro*, 72-hr AMD3100 treatment did
571 also not affect expression levels of these genes, and had no significant effect (although tendancy) on
572 the proportion of the SP (0.5% ± 0.3 *versus* 0.9% ± 0.2 in control; n=3; $p>0.05$). Of note, there was a
573 small increase in *Cxcr4* expression in the AMD3100-treated xenograft tumors (Fig. 4D); upregulation
574 of *Cxcr4* after AMD3100 treatment has also been reported in other tumors, supposedly due to
575 adaptation of the tumor to sustained Cxcr4 signal inhibition (Domanska *et al.* 2012). Together, EMT
576 genes – at least the ones analyzed - do not seem to be involved in the AMD3100-induced inhibition
577 of cell motile activity and of xenograft tumor growth (at least as examined after 20 days of
578 treatment). To search for possible other mechanisms of tumor growth reduction, cell viability and
579 proliferation were evaluated. Treatment of cultured AtT20 cells with AMD3100 results in a 2- to 3-
580 fold increase in dying/dead cells (from 2-4% in control to 8-11% after AMD3100 treatment; Fig. 4E).
581 In analogy, AMD3100 augments the number of AtT20 cells that go into apoptosis (about 2-fold; Fig.
582 4F). However, no difference was found (anymore) in the number of apoptotic cells after 20-day
583 AMD3100 treatment *in vivo* (data not shown). Treatment of cultured AtT20 cells with AMD3100 also
584 reduces the proportion of proliferating cells (from about 90 to 60% after 72 hr; Fig. 4G). From these
585 *in vitro* data, it is assumed that the tumor-growth inhibitory effect of AMD3100 at least partially
586 involves a reduction in cell viability and proliferation. From our data so far, there are no indications
587 yet that EMT is also implicated.
588

Pituitary tumorigenesis and pituitary stem cells

In addition to the finding of SOX2 expression in tumorsphere cells, our microarray analysis also revealed upregulated gene expression of *SOX2* in the adenoma pSP (>1.5-fold in 3 of the 5 human pituitary tumors analyzed; $p<0.05$). Interestingly, the AtT20 SP also shows higher expression of *Sox2* (as compared to the MP; Supplementary Fig. S6A). A comparable finding was observed in an additional pituitary tumor cell line, the rat lactosomatotrope GH3, also containing a SP (0.5% ± 0.05; n=18) (Supplementary Fig. S6A-B). Sox2 is a stemness factor which also marks the recently identified stem cells of the pituitary gland (Chen *et al.* 2009). In general, a link may exist between CSC/TSC of tumors in organs and the resident stem cells, as recently supported in several cancers (Barker *et al.* 2009; Llaguno *et al.* 2009; Zhu *et al.* 2009; Mulholland *et al.* 2010; Vankelecom & Gremeaux 2010; Clevers 2011; Lapouge *et al.* 2011; Chen *et al.* 2012; Schepers *et al.* 2012; Boumahdi *et al.* 2014; Vankelecom & Chen 2014; Vanner *et al.* 2014).

To further explore the pituitary stem cells in the gland's tumors, we turned to the dopamine D2 receptor knock out (*Drd2*$^{-/-}$) mouse model (Cristina *et al.* 2006). In the pituitary of *Drd2*$^{-/-}$ female mice, prolactinomas gradually develop starting from 6-8 months of age, as visible by MRI and after necropsy (Supplementary Fig. S7A). The CD31^{-}/CD45^{-} SP (pSP) proportion in the tumor-bearing AP from *Drd2*$^{-/-}$ mice (1.7% ± 0.3; n=5; Supplementary Fig. S7B) is higher than from heterozygous *Drd2*$^{+/-}$ (1.4% ± 0.6; n=2) and wildtype *Drd2*$^{+/+}$ control littermates (1.3% ± 0.2; n=2). Calculated to absolute cell numbers (see Materials and Methods), the *Drd2*$^{-/-}$ AP contains about 10-fold more pSP cells than the control mice (Fig. 5A). Similarly, the absolute number of colony-forming cells (also often used to *in-vitro* investigate TSC activity) is higher in *Drd2*$^{-/-}$ than *Drd2*$^{+/-}$ pituitaries (3.9-fold ± 0.7; n=3). In addition, colonies that develop from the *Drd2*$^{-/-}$ pituitary are generally larger in size and more smoothly shaped than the colonies from the heterozygous mice (Supplementary Fig. S7C).

We next examined the prolactinoma-bearing pituitary of *Drd2*$^{-/-}$ mice for Sox2^{+} cells. From countings in dissociated APs (see Materials and Methods), the absolute number of Sox2^{+} cells is higher in the *Drd2*$^{-/-}$ AP when compared to the wildtype gland (2.4-fold ± 0.6; n=3) (Fig. 5B). At least

615 part of the increase in Sox2^{+} cells is due to higher proliferative activity; whereas proliferating (Ki67^{+})
616 Sox2^{+} cells are virtually absent in wildtype Drd2$^{+/+}$ AP at the ages tested (6 to 12 months), double
617 Sox2^{+}/Ki67^{+} cells are more readily observed in Drd2$^{-/-}$ AP (Fig. 5C). Furthermore, as also seen before
618 (Chen *et al.* 2009; Fu *et al.* 2012; Gremeaux *et al.* 2012), Sox2-immunoreactive signal is not only
619 found in the expected location of the nucleus (nuclear-Sox2^{+} or nSox2^{+} cells), but some cells show
620 Sox2^{+} signal in the cytoplasm (cytoplasmic-Sox2^{+} or cSox2^{+} cells). The *Drd2*$^{-/-}$ cSox2^{+} cells show a
621 higher increase than the nSox2^{+} cells when compared to *Drd2*$^{+/+}$ wildtype pituitaries (3.1-fold ± 0.3
622 and 2.3-fold ± 0.7, respectively; Fig. 5B-C). *In situ*, Sox2^{+} cells in the *Drd2*$^{-/-}$ pituitary are found in the
623 marginal zone bordering the cleft, which is not different from wildtype (Fig. 5D and Supplementary
624 Fig. S7D). On top of this location, frequent clusters of Sox2^{+} cells are observed within the PRL^{+} tumor
625 cell mass in the *Drd2*$^{-/-}$ pituitary (Fig. 5D and Supplementary Fig. S7D). In the wildtype gland, Sox2^{+}
626 cell clusters are also observed spread within the endocrine AP parenchyma (Fig. 5D and
627 Supplementary Fig. S7D). Double Sox2^{+}/PRL^{+} cells were not observed in neither of the pituitary
628 phenotypes. Taken together, the number of Sox2^{+} cells clearly increases in *Drd2*$^{-/-}$ *versus* wildtype
629 pituitary, but their overall appearance in the putative stem cell niches seems not very different.
630

DISCUSSION

Adenomas represent the most frequent pathology of the pituitary gland. Despite extensive research, not much is known about the mechanisms underlying pituitary tumor pathogenesis.

In the present study, we demonstrate the existence of a SP in different models of pituitary tumor including human adenomas, mouse tumors and cell lines. During the last decade, a SP has been identified in many tumor types and cell lines, and was often found enriched in cells with CSC or CSC-like phenotype or activity (Patrawala *et al.* 2005; Wu & Alman 2008; Kato *et al.* 2010; Britton *et al.* 2012; Moti *et al.* 2014). The majority of these studies looked for CSC in malignant cancers. Our study is among the first to identify a SP in benign tumors (Wu *et al.* 2007) . The pituitary adenoma SP still represents a heterogeneous population, similar to the SP in other tumors as well as in healthy tissues (Pfister *et al.* 2005; Uezumi *et al.* 2006). In a previous study we also detected endothelial-type cells in the SP of the normal (mouse) pituitary; further purification led to the identification of pituitary stem cells (Chen *et al.* 2009). The endothelial-type SP cells of the pituitary tumors may represent a progenitor phenotype, driving angiogenesis during tumor expansion. Presence of endothelial progenitor cells in pituitary adenomas has indeed been suggested based on detection of CD133, CD34, NESTIN and VEGFR2 in non-hormonal and non-folliculostellate cells of the tumors (Yunoue *et al.* 2011). Of note, the expression picture distilled from the total adenoma SP was found to be largely reconfirmed in the purified $CD31^-/CD45^-$ SP (pSP). Also other studies have demonstrated that expression characteristics of minority CSC fractions can already surface in still mixed populations (Eppert *et al.* 2011).

Several genes upregulated in the (p)SP are associated with a 'tumor stemness' phenotype as also reported for the SP in other tumors (Patrawala *et al.* 2005; Wu & Alman 2008; Kato *et al.* 2010; Britton *et al.* 2012; Moti *et al.* 2014). In addition, the NOTCH, WNT and TGFβ/BMP pathways represent not only '(tumor) stemness' signaling systems but also regulatory circuits well known for their critical role in pituitary embryonic development (Zhu *et al.* 2007; Vankelecom 2010). Also the upregulated expression of *NOTCH2* may be remarkable in this sense because particularly this

member of the Notch receptor family is highly expressed in the progenitor cells of Rathke's pouch, the embryonic pituitary *anlage* (Zhu *et al.* 2007; Vankelecom 2010). This embryonic link may be in line with the idea that CSC recapitulate aspects of embryonic development. Also other studies suggested the involvement of NOTCH and WNT signaling in pituitary tumorigenesis as concluded from transcriptomic analysis of unfractionated adenomas (Moreno *et al.* 2005). Furthermore, the upregulation of *HIF2α* in the SP may be of importance; in other tumors like glioma, HIF2α regulates the tumorigenic capacity of the CSC fraction (Das *et al.* 2008). Hypoxia is known to stimulate CXCR4 expression (De Craene & Berx 2013) which is indeed found upregulated in the pituitary tumor (p)SP. In many cancer types CXCR4 has been advanced as a marker of CSC, and the pathway is known to play a role in CSC activity (Hermann *et al.* 2007; Vankelecom & Gremeaux 2010; Clevers 2011). Of further note, the epidermal growth factor receptor-associated protein-8 (EPS8) is also overexpressed in the pSP (4 of the 5 adenomas, $p<0.05$; Supplementary Table S8). This oncoprotein has previously been found upregulated in multiple pituitary tumor subtypes in which it mediates survival, proliferation and tumorigenicity (Xu *et al.* 2009a). Moreover, the accompanying receptor EGFR is also upregulated and is involved in tumor cell migration in some cancers (Hölsken *et al.* 2011). Finally, our expression data suggest that the PI3/Akt/mTOR/PTEN pathway is also enriched in the adenoma SP (data not shown). This pathway has been proposed to play a role in pituitary tumorigenesis (Dworakowska *et al.* 2009). Moreover, CXCR4 and PI3K/Akt are interconnected; it has been shown that paracrine/autocrine activation of CXCR4 signaling provokes Akt-mediated prosurvival of glioblastoma CSC (Rubin *et al.* 2003; Gatti *et al.* 2013).

It should be noticed that the expression pattern in the pSP does only minimally overlap with the set of genes (*CD133, NESTIN, CD90/THY1, OCT4, MSI, JAG2, NOTCH4, DLL1*) recently identified as upregulated in candidate pituitary TSC (so-called 'pituitary adenoma stem-like cells' or PASCs), which were obtained by sphere-like culture (Xu *et al.* 2009b). In our study, only *NOTCH4*, *DLL1* and *NESTIN* are found overexpressed, with *NOTCH4* and *DLL1* only upregulated in the total SP and not in the pSP. Moreover, expression levels of the multidrug transporter genes *BCRP1 (ABCG2)* and *MDR1 (ABCB1)*

were reported not to be upregulated in the PASCs (Xu *et al.* 2009b). These divergent results may be mainly explained by the use of cultured cells (Xu *et al.* 2009b) *versus* cells obtained directly from the tumor (present study) (further commented on in Vankelecom 2012; Vankelecom & Chen 2014).

In a recent study (Donangelo *et al.* 2014), candidate TSC were proposed to exist in pituitary tumors developing in $Rb^{+/-}$ mice. These tumors differ from typical pituitary adenomas (i.e. of the AP) since arising in the intermediate lobe (IL) of the gland. Stem cell antigen 1 (Sca1)-immunoreactive cells sorted from these IL tumors showed higher sphere-forming capacity when compared to the $Sca1^-$ cells, as well as increased expression of Sox2 and nestin, and tumor-growth advantage after injection of a high number of cells (10^5) into the brain striatum of NOD-SCID$^{IL2R\gamma-/-}$ mice. Before, we have shown that pituitary 'stemness' is rather accompanied by the absence of Sca1 and that Sca1 expression is mainly found in the endothelial fraction of the SP (Chen *et al.* 2009), later supported by the detection of Sca1 in progenitor cells of endothelial or mesenchymal origin in mouse pituitary cell lines (Mitsuishi *et al.* 2013). Thus, Sca1 expression may represent a difference in the signature of the IL tumor TSC and the normal pituitary stem cells. Alternatively, $Sca1^+$ cells from the IL tumors may also include endothelial progenitor cells ($CD31^+$ cells were not removed from the $Sca1^+$ fraction) which would facilitate tumor xenograft development by providing angiogenic support, and which may be an (additional) explanation for the tumor-growth advantage. Similar to our findings, the $Sca1^+$ fraction did not fully retrieve the tumorigenic activity and $Sca1^-$ cells also formed tumors (although to a lower extent). Intriguingly, in the majority of the xenograft tumors derived from the $Sca1^+$ cell population, no $Sca1^+$ cells could be detected anymore, which does not exactly fit with the definition of self-renewing CSC. It should also be remarked that Sca1 cannot be employed as a (potential) TSC marker in human pituitary adenomas since this gene (product) does not exist in man.

In contrast to the highly penetrant $Rb^{+/-}$ IL tumors (Donangelo *et al.* 2014), benign human pituitary adenomas (transplanted sc or subrenally) did not expand in mice whatever the mouse grade of immunodeficiency. Xu *et al.* (2009b) reported 'growth and reconstitution of the original tumor' from their PASC spheroids (as analyzed for 1 GH-A) when implanted in the forebrain of NOD/SCID

709 mice, but no clearly demarcated tumor or expansion was shown (further reviewed in Vankelecom
710 2012; Vankelecom & Chen 2014).

711 Since the standard xenograft assay did not work starting form benign human pituitary adenoma,
712 we further turned to *in vitro* TSC assays and to the well-established pituitary tumor AtT20 cell line.
713 Cultured cell lines are often used as complementary paradigms to study (candidate) CSC. Moreover,
714 in cell lines of multiple cancer types, the SP has been found to enrich for authentic or candidate CSC
715 (Patrawala *et al.* 2005; Wu & Alman 2008; Kato *et al.* 2010; Britton *et al.* 2012). First, we discovered
716 that human pituitary adenomas contain self-renewing sphere-forming cells that express the
717 stemness markers Sox2 and nestin, and that the sphere-initiating cells segregate to the pSP. In
718 addition, the AtT20 cell line also contains a SP which was found to enrich for cells that are more
719 tumorigenic (i.e. grow faster and larger tumors) than MP cells, that better reconstitute the tumor's
720 original heterogeneity (SP/MP profile) - a further property of CSC -, and that express CSC-associated
721 genes. The segregation of tumorigenic activity in the SP is not absolute as also observed in various
722 other studies on CSC (Boumahdi *et al.* 2014; Vanner *et al.* 2014) and in the $Rb^{+/-}$ IL tumors as
723 mentioned above (Donangelo *et al.* 2014).

724 The (p)SP identified also displays an expression pattern supportive of EMT occurring in that
725 tumor compartment. In recent studies, CSC and EMT have been linked in that EMT acts as a major
726 driver of CSC generation and activity (Mani *et al.* 2008; Morel *et al.* 2008; Kong *et al.* 2010; Pirozzi *et*
727 *al.* 2011; Yoon *et al.* 2012; De Craene & Berx 2013). In addition to being an argument in favor of the
728 CSC(-like) phenotype of the pSP, the detection of EMT may also have implications for understanding
729 pituitary tumor behavior. In several cancers, EMT, or EMT-driven CSC, are involved in expansion,
730 invasion, resistance to hostile conditions (including therapy) and recurrence (Mani *et al.* 2008; Morel
731 *et al.* 2008; Bertran *et al.* 2009; Kong *et al.* 2010; Pirozzi *et al.* 2011; De Craene & Berx 2013). The GO
732 enrichment picture including gene clusters associated with cell motility and migration, as well as the
733 expression of chemotactic receptors like *CXCR4* in the adenoma pSP further supports the migratory
734 capacity. Noteworthy, highest relative expression levels in the pSP (and highest differences in pSP

735 *versus* pMP) of the EMT-associated genes *ZEB2, SNAI2* and *TWIST1* were found in the adenoma
736 sample with the most aggressive character regarding invasion of neighbouring structures (PA 40 in
737 Table 1). On the other hand, from the data of a limited number of tumors assessed for invasive
738 character (i.e. PA03, 06, 07, 10, 15, 17, 19, 20, 22, 23, 33, 34, 35, 38, 40), no correlation emerged
739 (yet) between invasiveness and SP proportion. The pSP compartment also expresses angiogenic
740 factors which may suggest that TSC drive tumor angiogenesis to support the growth of the tumor.
741 CSC may also contribute to neovascularization through transdifferentiation to endothelial cells as has
742 been reported in glioblastoma (Dong *et al.* 2011). Processes such as EMT, angiogenesis and hypoxia
743 are known to contribute to maintenance and regulation of CSC in interaction with their
744 microenvironment.

745 Because human pituitary adenoma fails to grow not only *in vivo* but also *in vitro* (Hofland &
746 Lamberts 2002), EMT was further studied in the AtT20 cell line. The TGFβ pathway is known as an
747 important regulator of EMT (Bertran *et al.* 2009; Pirozzi *et al.* 2011; De Craene & Berx 2013).
748 Although TGFβ activation stimulated expression of some EMT-regulatory and 'stemness'-associated
749 genes, treatment of AtT20 did not enhance EMT-linked cell motility, neither did pretreatment induce
750 faster or more pronounced xenograft tumor formation. Of note, the impact of the *in vitro*
751 pretreatment may fade away during *in vivo* growth. In general, TGFβ is known to play a dual role in
752 tumor pathogenesis: it may not only promote tumor progression (angiogenesis, invasion, metastasis)
753 by stimulating tumorigenic activity and EMT (Mani *et al.* 2008; Bertran *et al.* 2009; Pirozzi *et al.* 2011;
754 De Craene & Berx 2013) but may also inhibit tumor growth by reducing cell proliferation (Ramsdell
755 1991; Tirino *et al.* 2013). We indeed observed a small tendency towards slower tumor growth after
756 pretreatment of the AtT20 cells with TGFβ1 (see Supplementary Fig. S5C). Furthermore, it should be
757 mentioned that AtT20 cells already display some mesenchymal character in basal conditions as
758 concluded from their spindle-shaped morphology and their basic motility in the scratch assay (data
759 not shown), which may explain the limitation to supplementarily activate a mesenchymal phenotype.
760 Regarding the CXCR4 pathway as the second EMT-regulatory system tested, inhibition leads to

761 reduction of AtT20 cell motility and of tumor growth. The latter finding is in line with a previous
762 study showing that anti-CXCR4 treatment suppresses primary brain tumor growth, and that
763 treatment of mice with AMD3100 results in decreased proliferation and invasion of the xenografted
764 brain tumors, and in better survival of the animals (Rubin *et al.* 2003). In addition, activation of
765 CXCR4 has been shown to stimulate cell proliferation in human pituitary adenoma cultures (Barbieri
766 *et al.* 2008). Here, we show that the Cxcr4 pathway is involved in pituitary tumor growth *in vivo*.
767 AMD3100 was found to induce AtT20 cell death and apoptosis, and to reduce cell proliferation (as
768 analyzed *in vitro*), similar to findings by others in pituitary and other tumors (Barbieri *et al.* 2008;
769 Gatti *et al.* 2013). Whether EMT is (also) implicated in the growth-inhibitory effect of AMD3100, is
770 not clear yet; expression of the tested selection of EMT genes was not affected after long-term
771 treatment *in vivo* (20 days) or short-term exposure *in vitro* (72 hr). EMT-associated genes different
772 from the ones analyzed may still be involved (as e.g. described in breast CSC; Yoon *et al.* 2012).
773 Neither activation of the TGFβ pathway nor inhibition of the Cxcr4 pathway significantly affected the
774 SP proportion, although effects may be small and absence of an effect on proportion does not
775 exclude a possible effect on the (molecular) activation status of the SP cells. Further studies are
776 needed to shed more light on the mechanisms.

777 An important question in cancer research concerns the link of tumorigenesis (and CSC) with the
778 tissue's own stem cells. In several types of cancer, it has been shown that tissue stem cells are at the
779 origin of tumors and/or of CSC (Barker *et al.* 2009; Llaguno *et al.* 2009; Zhu *et al.* 2009; Mulholland *et*
780 *al.* 2010; Lapouge *et al.* 2011; Chen *et al.* 2012; Schepers *et al.* 2012; Boumahdi *et al.* 2014; Vanner *et*
781 *al.* 2014). On the other hand, stem cells may not directly be involved, but may become activated
782 when a tumorigenic 'assault' is occurring in their tissue (Vankelecom & Gremeaux 2010; Vankelecom
783 & Chen 2014). Here, we observed that the pSP, the $Sox2^{+}$ and the colony-forming cells are increased
784 in number when tumors are present in the pituitary, as analyzed in *Drd2*$^{-/-}$ mice in which
785 prolactinomas develop within their natural microenvironment. Our findings suggest activation of the
786 pituitary stem cell compartment during tumorigenesis with a rise in cell number. It should be noted

that the populations identified may comprise both the 'normal' pituitary stem cells and the (potentially stem cell-derived) TSC or TSC-like cells. At present, it is not possible to distinguish between both on the basis of the properties analyzed (SP, Sox2 expression, colony formation). The fact that cell numbers and increments are not identical among the 3 populations (pSP, $Sox2^+$ and colony-forming) suggests that they do not fully overlap, as has also been observed before (Chen *et al.* 2009; Fu *et al.* 2012). Moreover, more than one (cancer) stem cell population has also been detected in other tissues and tumors (see e.g. Zhu *et al.* 2014). The finding that these populations expand in number may indicate that the stem cells react during tumorigenesis and that they may play a role in the pathogenic process. Of note, the higher increase in cytoplasmic-$Sox2^+$ cells in the tumorous pituitary might support a higher differentiation rate towards tumor PRL^+ cells (Chen *et al.* 2009; Fu *et al.* 2012; Gremeaux *et al.* 2012). In addition, $Sox2^+$ cell clusters were often observed within the PRL^+ tumor cell masses, although they also occur scattered over the parenchyma in the normal AP. Whether existing clusters are entrapped during tumor formation, or whether they play a more active role in the tumorigenic process, either directly (as origin) or indirectly (as tumor-inducing or -tropic), needs to be further clarified (e.g. by lineage tracing). In a recent study, lineage tracing did not detect a direct link of descent between transgenically Wnt/β-catenin-induced craniopharyngioma in the pituitary and the $Sox2^+$ stem cells. Instead, findings suggested that the $Sox2^+$ stem cells rather act as paracrine tumor-activating cells (Andoniadou *et al.* 2013). Adamantinomatous craniopharyngioma is a typically pediatric tumor likely originating from ectopic remnants of Rathke's pouch, and thus different from the typical AP tumors. The transcription factor Sox2 itself may also play a role in pituitary tumorigenesis, e.g. when not properly shut down by the tumor suppressor p27 (at least as demonstrated for IL tumors; reviewed in Vankelecom and Chen, 2014). In addition, Sox2 can act as an oncogene in tissues where it is expressed in the putative stem cells (e.g. lung, oesophagus and skin) (Arnold *et al.* 2011; Boumahdi *et al.* 2014). Also overexpression of other pituitary stem cell factors (like Prop1) from the early Rathke's pouch state onwards, may lead to tumor formation in the gland (reviewed in Vankelecom and Chen, 2014). Again, Prop1 is not found within the tumors but in

non-neoplastic regions surrounding the lesions, suggesting that Prop1 overexpression does not generate tumor-driving stem cells but rather trophically supporting cells.

In conclusion of our study, we identified a SP in pituitary tumor displaying TSC-associated molecular and functional characteristics. Identification of this cell population may eventually help to better understand pituitary tumor pathogenesis, and may have an impact on clinical management of the disease. The global molecular profile of the pSP may thereby serve as a valuable source to identify potentially interesting therapeutic targets for further examination.

DECLARATION OF INTERESTS

The authors declare that there is no conflict of interest that could be perceived as prejudicing the impartiality of the research report.

FUNDING

This work has been supported by research grants from the KU Leuven (Research Fund, BOF) and from the Fund for Scientific Research (FWO) Flanders (Belgium), by a joint research grant between FWO and the Ministry of Science and Technology of China (MOST; 2012DFG32000), by a joint travel grant between FWO and the Ministry of Science, Technology and Productive Innovation (MinCyt) of Argentina, and by collaborative efforts in the context of grants from the National Natural Science Foundation (NSF) of China (30500248 and 81300641). FM and HR obtained a PhD Fellowship from the IWT (Agency for Innovation by Science and Technology; Flanders, Belgium), and LG from the FWO.

ACKNOWLEDGMENTS

We dedicate this paper to Vik Van Duppen (Stem Cell Institute – SCIL, KU Leuven), our FACS expert who tragically passed away in 2013. Without his proficient help, SP analysis would never have been developed to a successful technique in our laboratory. We also thank Rob Van Rossom (SCIL) for his help with FACS analysis and sorting, and the VIB Nucleomics Core (www.nucleomics.be) for their expert assistance in microarray analysis. We are further indebted to Yvonne Van Goethem (HV lab) for technical assistance, to Jasper Wouters en Anke Van den broeck (former PhD students in the HV lab) for their valuable input and discussions, and to the Department of Imaging and Pathology and Biobank (Dr. Sciot; University Hospitals Leuven). We also thank the 'Molecular Small Animal Imaging Centre' (MoSAIC, KU Leuven) for their valued guidance in pituitary imaging using MRI, the CIC for use of the Zeiss confocal microscope and InfraMouse (KU Leuven-VIB, Hercules type 3 grant) for use of the Leica microscope.

REFERENCES

Andoniadou CL, Matsushima D, Mousavy Gharavy SN, Signore M, Mackintosh AI, Schaeffer M, Gaston-Massuet C, Mollard P, Jacques TS, Le Tissier P *et al.* 2013 Sox2(+) stem/progenitor cells in the adult mouse pituitary support organ homeostasis and have tumor-inducing potential. *Cell Stem Cell* **13** 433–445. (doi:10.1016/j.stem.2013.07.004)

Arnold K, Sarkar A, Yram MA, Polo JM, Sengupta S, Seandel M, Geijsen N & Hochedlinger K 2011 Sox2+ adult stem/progenitor cells are important for tissue regeneration and survival of mice. *Cell Stem Cell* **9** 317–329. (doi:10.1016/j.stem.2011.09.001.Sox2)

Barbieri F, Bajetto A, Stumm R, Pattarozzi A, Porcile C, Zona G, Dorcaratto A, Ravetti J-L, Minuto F, Spaziante R *et al.* 2008 Overexpression of stromal cell-derived factor 1 and its receptor CXCR4 induces autocrine/paracrine cell proliferation in human pituitary adenomas. *Clinical Cancer Research : An Official Journal of the American Association for Cancer Research* **14** 5022–5032. (doi:10.1158/1078-0432.CCR-07-4717)

Barker N, Ridgway R a, van Es JH, van de Wetering M, Begthel H, van den Born M, Danenberg E, Clarke AR, Sansom OJ & Clevers H 2009 Crypt stem cells as the cells-of-origin of intestinal cancer. *Nature.* **457** 608–611.

Bertran E, Caja L, Navarro E, Sancho P, Mainez J, Murillo MM, Vinyals A, Fabra A & Fabregat I 2009 Role of CXCR4/SDF-1 alpha in the migratory phenotype of hepatoma cells that have undergone epithelial-mesenchymal transition in response to the transforming growth factor-beta. *Cellular Signalling* **21** 1595–1606. (doi:10.1016/j.cellsig.2009.06.006)

Boumahdi S, Driessens G, Lapouge G, Rorive S, Nassar D, Le Mercier M, Delatte B, Caauwe A, Lenglez S, Nkusi E *et al.* 2014 SOX2 controls tumour initiation and cancer stem-cell functions in squamous-cell carcinoma. *Nature*. (doi:10.1038/nature13305)

Britton KM, Eyre R, Harvey IJ, Stemke-Hale K, Browell D, Lennard TWJ & Meeson a P 2012 Breast cancer, side population cells and ABCG2 expression. *Cancer Letters* **323** 97–105. (doi:10.1016/j.canlet.2012.03.041)

Chen J, Hersmus N, Van Duppen V, Caesens P, Denef C & Vankelecom H 2005 The adult pituitary contains a cell population displaying stem/progenitor cell and early embryonic characteristics. *Endocrinology* **146** 3985–3998. (doi:10.1210/en.2005-0185)

Chen J, Gremeaux L, Fu Q, Liekens D, Van Laere S & Vankelecom H 2009 Pituitary progenitor cells tracked down by side population dissection. *Stem Cells (Dayton, Ohio)* **27** 1182–1195. (doi:10.1002/stem.51)

Chen J, Li Y, Yu T-S, McKay RM, Burns DK, Kernie SG & Parada LF 2012 A restricted cell population propagates glioblastoma growth after chemotherapy. *Nature* **488** 522–526. (doi:10.1038/nature11287)

Clevers H 2011 The cancer stem cell: premises, promises and challenges. *Nature Medicine* **17** 313–319. (doi:10.1038/nm.2304)

De Craene B & Berx G 2013 Regulatory networks defining EMT during cancer initiation and progression. *Nature Reviews. Cancer* **13** 97–110. (doi:10.1038/nrc3447)

Cristina C, Rubinstein M, Low MJ & Becu-Villalobos D 2006 Dopaminergic D2 Receptor Knockout Mouse: An Animal Model of Prolactinoma. *Frontiers of Hormone Research* **35** 50–63.

Daly AF, Tichomirowa M a & Beckers A 2009 The epidemiology and genetics of pituitary adenomas. *Best Practice & Research. Clinical Endocrinology & Metabolism* **23** 543–554. (doi:10.1016/j.beem.2009.05.008)

Das B, Tsuchida R, Malkin D, Koren G, Baruchel S & Yeger H 2008 Hypoxia enhances tumor stemness by increasing the invasive and tumorigenic side population fraction. *Stem Cells (Dayton, Ohio)* **26** 1818–1830. (doi:10.1634/stemcells.2007-0724)

Domanska UM, Timmer-Bosscha H, Nagengast WB, Munnink THO, Kliphuis NM & Huls G 2012 CXCR4 Inhibition with AMD3100 Sensitizes Prostate Cancer to docetaxel chemotherapy. *Neoplasia* **14** 709–718. (doi:10.1593/neo.12324)

Donangelo I, Ren S-G, Eigler T, Svendsen C & Melmed S 2014 Sca1-positive murine pituitary adenoma cells show tumor growth advantage. *Endocrine-Related Cancer* **21** 203–216. (doi:10.1530/ERC-13-0229)

Dong J, Zhao Y, Huang Q, Fei X, Diao Y, Shen Y, Xiao H, Zhang T, Lan Q & Gu X 2011 Glioma stem/progenitor cells contribute to neovascularization via transdifferentiation. *Stem Cell Reviews* **7** 141–152. (doi:10.1007/s12015-010-9169-7)

Dworakowska D, Wlodek E, Leontiou CA, Igreja S, Cakir M, Teng M, Prodromou N, Góth MI, Grozinsky-Glasberg S, Gueorguiev M *et al.* 2009 Activation of RAF/MEK/ERK and PI3K/AKT/mTOR pathways in pituitary adenomas and their effects on downstream effectors. *Endocrine-Related Cancer* **16** 1329-1338.

Eppert K, Takenaka K, Lechman ER, Waldron L, Nilsson B, van Galen P, Metzeler KH, Poeppl A, Ling V, Beyene J *et al.* 2011 Stem cell gene expression programs influence clinical outcome in human leukemia. *Nature Medicine* **17** 1086–1093. (doi:10.1038/nm.2415)

Fu Q, Gremeaux L, Luque RM, Liekens D, Chen J, Buch T, Waisman A, Kineman R & Vankelecom H 2012 The Adult Pituitary Shows Stem/Progenitor Cell Activation in Response to Injury and Is Capable of Regeneration. *Endocrinology* **153** 1–12. (doi:10.1210/en.2012-1152)

Galland F, Lacroix L, Saulnier P, Dessen P, Meduri G, Bernier M, Gaillard S, Guibourdenche J, Fournier T, Evain-Brion D *et al.* 2010 Differential gene expression profiles of invasive and non-invasive non-functioning pituitary adenomas based on microarray analysis. *Endocrine-Related Cancer* **17** 361–371. (doi:10.1677/ERC-10-0018)

Gatti M, Pattarozzi A, Bajetto A, Würth R, Daga A, Fiaschi P, Zona G, Florio T & Barbieri F 2013 Inhibition of CXCL12/CXCR4 autocrine/paracrine loop reduces viability of human glioblastoma stem-like cells affecting self-renewal activity. *Toxicology* **314** 209–220. (doi:10.1016/j.tox.2013.10.003)

Gremeaux L, Fu Q, Chen J & Vankelecom H 2012 Activated phenotype of the pituitary stem/progenitor cell compartment during the early-postnatal maturation phase of the gland. *Stem Cells and Development* **20** 801–813.

Hermann PC, Huber SL, Herrler T, Aicher A, Ellwart JW, Guba M, Bruns CJ & Heeschen C 2007 Distinct populations of cancer stem cells determine tumor growth and metastatic activity in human pancreatic cancer. *Cell Stem Cell* **1** 313–323. (doi:10.1016/j.stem.2007.06.002)

Hofland LJ & Lamberts W 2002 Pituitary gland tumors. In *Human Cell Culture*, pp 149–159. (doi:10.1007/s00292-003-0625-x)

Hölsken A, Gebhardt M, Buchfelder M, Fahlbusch R, Blümcke I & Buslei R 2011 EGFR signaling regulates tumor cell migration in craniopharyngiomas. *Clinical Cancer Research : An Official Journal of the American Association for Cancer Research* **17** 4367–4377. (doi:10.1158/1078-0432.CCR-10-2811)

Kato K, Takao T, Kuboyama A, Tanaka Y, Ohgami T, Yamaguchi S, Adachi S, Yoneda T, Ueoka Y, Kato K *et al.* 2010 Endometrial cancer side-population cells show prominent migration and have a potential to differentiate into the mesenchymal cell lineage. *The American Journal of Pathology* **176** 381–392. (doi:10.2353/ajpath.2010.090056)

Kong D, Banerjee S, Ahmad A, Li Y, Wang Z, Sethi S & Sarkar FH 2010 Epithelial to mesenchymal transition is mechanistically linked with stem cell signatures in prostate cancer cells. *PloS One* **5** e12445. (doi:10.1371/journal.pone.0012445)

Lapouge G, Youssef KK, Vokaer B, Achouri Y, Michaux C, Sotiropoulou P a & Blanpain C 2011 Identifying the cellular origin of squamous skin tumors. *Proceedings of the National Academy of Sciences of the United States of America* **108** 7431–7436. (doi:10.1073/pnas.1012720108)

Llaguno SA, Chen J, Kwon C, Jackson EL, Li Y, Burns DK, *et al*. 2009 Malignant Astrocytomas Originate from Neural Stem/Progenitor Cells in a Somatic Tumor Suppressor Mouse Model. *Cancer Cell* **15** 45–56.

Mani S a, Guo W, Liao M-J, Eaton EN, Ayyanan A, Zhou AY, Brooks M, Reinhard F, Zhang CC, Shipitsin M *et al.* 2008 The epithelial-mesenchymal transition generates cells with properties of stem cells. *Cell* **133** 704–715. (doi:10.1016/j.cell.2008.03.027)

Melmed S 2011 Pathogenesis of pituitary tumors. *Nature Reviews. Endocrinology* **7** 257–266. (doi:10.1038/nrendo.2011.40)

Mitsuishi H, Kato T, Chen M, Cai L-Y, Yako H, Higuchi M, Yoshida S, Kanno N, Ueharu H & Kato Y 2013 Characterization of a pituitary-tumor-derived cell line, TtT/GF, that expresses Hoechst efflux ABC transporter subfamily G2 and stem cell antigen 1. *Cell and Tissue Research* **354** 563–572. (doi:10.1007/s00441-013-1686-7)

Morel A-P, Lièvre M, Thomas C, Hinkal G, Ansieau S & Puisieux A 2008 Generation of breast cancer stem cells through epithelial-mesenchymal transition. *PloS One* **3** e2888. (doi:10.1371/journal.pone.0002888)

Moreno CS, Evans C-O, Zhan X, Okor M, Desiderio DM & Oyesiku NM 2005 Novel molecular signaling and classification of human clinically nonfunctional pituitary adenomas identified by gene

961 expression profiling and proteomic analyses. *Cancer Research* **65** 10214–10222.
962 (doi:10.1158/0008-5472.CAN-05-0884)

963 Moti N, Malcolm T, Hamoudi R, Mian S, Garland G, Hook CE, Burke G a a, Wasik M a, Merkel O,
964 Kenner L *et al.* 2014 Anaplastic large cell lymphoma-propagating cells are detectable by side
965 population analysis and possess an expression profile reflective of a primitive origin. *Oncogene*
966 1–10. (doi:10.1038/onc.2014.112)

967 Mulholland DJ, Xin L, Morim A, Lawson D, Witte O, Wu H 2010 LSC Stem/Progenitors Are Tumor
968 Initiating Cells in the Pten Null Prostate Cancer Model. *Cancer Research* **69** 8555–8562.

969 Patrawala L, Calhoun T, Schneider-Broussard R, Zhou J, Claypool K & Tang DG 2005 Side population is
970 enriched in tumorigenic, stem-like cancer cells, whereas ABCG2+ and ABCG2- cancer cells are
971 similarly tumorigenic. *Cancer Research* **65** 6207–6219. (doi:10.1158/0008-5472.CAN-05-0592)

972 Pfister O, Mouquet F, Jain M, Summer R, Helmes M, Fine A, Colucci WS & Liao R 2005 CD31- but Not
973 CD31+ cardiac side population cells exhibit functional cardiomyogenic differentiation.
974 *Circulation Research* **97** 52–61. (doi:10.1161/01.RES.0000173297.53793.fa)

975 Pirozzi G, Tirino V, Camerlingo R, Franco R, La Rocca A, Liguori E, Martucci N, Paino F, Normanno N &
976 Rocco G 2011 Epithelial to mesenchymal transition by TGFβ-1 induction increases stemness
977 characteristics in primary non small cell lung cancer cell line. *PloS One* **6** e21548.
978 (doi:10.1371/journal.pone.0021548)

979 Ramsdell JS 1991 Transforming growth factor-alpha and -beta are potent and effective inhibitors of
980 GH4 pituitary tumor cell proliferation. line. *Endocrinology* **128** 1981-1990.

981 Rubin JB, Kung AL, Klein RS, Chan J a, Sun Y, Schmidt K, Kieran MW, Luster AD & Segal R a 2003 A
982 small-molecule antagonist of CXCR4 inhibits intracranial growth of primary brain tumors.
983 *Proceedings of the National Academy of Sciences of the United States of America* **100** 13513–
984 13518. (doi:10.1073/pnas.2235846100)

985 Schepers AG, Snippert HJ, Stange DE, van den Born M, van Es JH, van de Wetering M & Clevers H
986 2012 Lineage tracing reveals Lgr5+ stem cell activity in mouse intestinal adenomas. *Science*
987 *(New York, N.Y.)* **337** 730–735. (doi:10.1126/science.1224676)

988 Taguchi T, Takao T, Iwasaki Y, Nishiyama M, Asaba K & Hashimoto K 2006 Suppressive effects of
989 dehydroepiandrosterone and the nuclear factor-kappaB inhibitor parthenolide on corticotroph
990 tumor cell growth and function in vitro and in vivo. *The Journal of Endocrinology* **188** 321–331.
991 (doi:10.1677/joe.1.06418)

992 Tirino V, Camerlingo R, Bifulco K, Irollo E, Montella R, Paino F, Sessa G, Carriero M V, Normanno N,
993 Rocco G *et al.* 2013 TGF-β1 exposure induces epithelial to mesenchymal transition both in CSCs
994 and non-CSCs of the A549 cell line, leading to an increase of migration ability in the CD133+
995 A549 cell fraction. *Cell Death & Disease* **4** e620. (doi:10.1038/cddis.2013.144)

996 Uezumi A, Ojima K, Fukada S, Ikemoto M, Masuda S, Miyagoe-Suzuki Y & Takeda S 2006 Functional
997 heterogeneity of side population cells in skeletal muscle. *Biochemical and Biophysical Research*
998 *Communications* **341** 864–873. (doi:10.1016/j.bbrc.2006.01.037)

Vankelecom H 2010 Pituitary stem/progenitor cells: embryonic players in the adult gland? *The European Journal of Neuroscience* **32** 2063–2081. (doi:10.1111/j.1460-9568.2010.07523.x)

Vankelecom H 2012 Pituitary stem cells drop their mask. *Current Stem Cell Research & Therapy* **7** 36–71.

Vankelecom H & Chen J 2014 Pituitary stem cells: where do we stand? *Molecular and Cellular Endocrinology* **385** 2–17. (doi:10.1016/j.mce.2013.08.018)

Vankelecom H & Gremeaux L 2010 Stem cells in the pituitary gland: A burgeoning field. *General and Comparative Endocrinology* **166** 478–488. (doi:10.1016/j.ygcen.2009.11.007)

Vanner RJ, Remke M, Gallo M, Selvadurai HJ, Coutinho F, Lee L, Kushida M, Head R, Morrissy S, Zhu X *et al.* 2014 Quiescent Sox2(+) Cells Drive Hierarchical Growth and Relapse in Sonic Hedgehog Subgroup Medulloblastoma. *Cancer Cell* **26** 33–47. (doi:10.1016/j.ccr.2014.05.005)

Wu C & Alman B a 2008 Side population cells in human cancers. *Cancer Letters* **268** 1–9. (doi:10.1016/j.canlet.2008.03.048)

Wu C, Wei Q, Utomo V, Nadesan P, Whetstone H, Kandel R, Wunder JS & Alman B a 2007 Side population cells isolated from mesenchymal neoplasms have tumor initiating potential. *Cancer Research* **67** 8216–8222. (doi:10.1158/0008-5472.CAN-07-0999)

Xu M, Shorts-Cary L, Knox AJ, Kleinsmidt-DeMasters B, Lillehei K & Wierman ME 2009a Epidermal growth factor receptor pathway substrate 8 is overexpressed in human pituitary tumors: role in proliferation and survival. *Endocrinology* **150** 2064–2071. (doi:10.1210/en.2008-1265)

Xu Q, Yuan X, Tunici P, Liu G, Fan X, Xu M, Hu J, Hwang JY, Farkas DL, Black KL *et al.* 2009b Isolation of tumour stem-like cells from benign tumours. *British Journal of Cancer* **101** 303–311. (doi:10.1038/sj.bjc.6605142)

Yoon C-H, Kim M-J, Lee H, Kim R-K, Lim E-J, Yoo K-C, Lee G-H, Cui Y-H, Oh YS, Gye MC *et al.* 2012 PTTG1 oncogene promotes tumor malignancy via epithelial to mesenchymal transition and expansion of cancer stem cell population. *The Journal of Biological Chemistry* **287** 19516–19527. (doi:10.1074/jbc.M111.337428)

Yunoue S, Arita K, Kawano H, Uchida H, Tokimura H & Hirano H 2011 Identification of CD133+ cells in pituitary adenomas. *Neuroendocrinology* **94** 302–312. (doi:10.1159/000330625)

Zhu X, Gleiberman AS & Rosenfeld MG 2007 Molecular physiology of pituitary development: signaling and transcriptional networks. *Physiological Reviews* **87** 933–963. (doi:10.1152/physrev.00006.2006)

Zhu L, Gibson P, Currle DS, Tong Y, Richardson RJ, Bayazitov IT, Poppleton H, Zakharenko S, Ellison DW & Gilbertson RJ 2009 Prominin 1 marks intestinal stem cells that are susceptible to neoplastic transformation. Nature **457**: 603-607.

Zhu Z, Khan MA, Weiler M, Blaes J, Jestaedt L, Geibert M, Zou P, Gronych J, Bernhardt O, Korshunov A *et al.* 2014 Targeting Self-Renewal in High-Grade Brain Tumors Leads to Loss of Brain Tumor Stem Cells and Prolonged Survival. *Cell Stem Cell* **15** 185–198. (doi:10.1016/j.stem.2014.04.007)

1036

FIGURE LEGENDS

Fig. 1. Identification and characterization of the side population (SP) in human pituitary adenomas

(A) Dot plots of dual-wavelength FACS analysis of human pituitary adenoma cells after incubation with Hoechst33342 alone (*left*), or together with verapamil (*right*). The SP (*black*) and MP (*white*) are gated and SP proportions are indicated. A representative example is shown.

(B) Boxplot of SP proportions obtained from NF-A (n=33) and GH-A (n=20) as well as from all samples taken together (n=60). Minimum and maximum values (*whiskers*) and outliers (*dots*) are indicated.

(C) Dot plots of FACS analysis of human pituitary adenoma cells after incubation with Hoechst33342 and immunostaining for CD31 and CD45. The $CD31^+$, $CD45^+$ and $CD31^-/CD45^-$ cells within the SP are also shown (*inset*).

(D) Percentage of $CD31^+$ *(upper panel)* and $CD45^+$ cells *(lower panel*) within the SP *versus* the SP proportion within the pituitary adenomas analyzed (n=37 and 31, respectively).

(E) Expression analysis by RT-qPCR of a selection of markers identified as differentially expressed in the pituitary adenoma $CD31^-/CD45^-$ SP (pSP) *versus* the pMP by microarray analysis. Bars indicate mean of fold expression pSP/pMP ± SEM (n=7 pituitary adenomas); *, $p<0.05$.

Fig. 2. Human pituitary tumors contain sphere-forming cells segregating to the pSP

(A) Smooth-edged spheres (*arrows*) develop in cultures of total pituitary adenoma cells, clearly distinct from clumps of cells sticking together (*arrowheads*).

(B) Examples of spheres at higher magnification.

(C) Spheres (*arrow*) show Sox2 immunofluorescent signal (*red*) whereas clumps do not (*arrowheads*). Nuclei are stained with ToPro3. A representative example is shown (*left*: light-microscopic image; *right*: overlay).

(D) Secondary spheres (*arrows*) form after re-seeding the dissociated primary sphere cells.

(E) Example of a secondary sphere at higher magnification.

(F) Third-generation spheres (*arrow*) develop after re-seeding the dissociated second-generation sphere cells.

(G) Spheres develop from pSP cells of pituitary adenoma, although their number is low. In pMP cell cultures, only clumps of cells are observed (*inset*).

All pictures were taken at 7 days of culture. Scale bar: 50µm.

Fig. 3. Identification and characterization of the SP in the AtT20 pituitary tumor cell line

(A) Dot plots of dual-wavelength FACS analysis of AtT20 cells after incubation with Hoechst33342 alone (*left*), or together with verapamil (*right*). The SP (*black*) and MP (*white*) are gated and SP proportions are indicated. A representative example is shown.

(B) *Cd44* and *Cxcr4* gene expression in the SP and MP of AtT20 cells in culture, as determined by RT-qPCR. Bars show mean of fold SP/MP ± SEM (n=3); *, $p<0.05$.

(C) Volume of xenograft tumors grown in SCID mice as measured at day 40 (d40) and d47 after sc injection of the indicated number of AtT20 SP cells (*black*) and MP cells (*grey*). Bars show mean ± SEM (5 mice for 10 000 cells, and 4 mice for 5000 and 1000 cells; injected in 2 or 3 independent experiments; see Supplementary Fig. S5B); *, $p<0.05$.

Fig. 4. Involvement of the TGFβ and Cxcr4 pathways in EMT-/TSC-associated properties of the AtT20 pituitary tumor cell line

(A) Gene expression in TGFβ1-treated (72 hr) and -untreated AtT20 cells as determined by RT-qPCR. Bars show mean of fold TGFβ1/control ± SEM (n=3); *, $p<0.05$.

(B) Effect of TGFβ1 and AMD3100 on the motility of AtT20 cells. Light-microscopic pictures of the AtT20 cell culture after applying a scratch 'wound', treated or not (control) with TGFβ1 or AMD3100 for the indicated time period. Representative examples are shown. Scale bar: 100µm. The '% open

area' was determined with TScratch software in the cultures without compound (*black*), or with TGFβ1 (*grey*) or AMD3100 (*dark grey*). Bars show mean ± SEM (n=4); *, p<0.05.

(C) Effect of the Cxcr4-antagonist AMD3100 on AtT20 tumor growth. Immunodeficient SCID mice with growing AtT20-derived sc tumors were treated with intratumoral injections of AMD3100 (*grey*) or vehicle (PBS; *black*) starting from day 21 (*arrow*) after sc AtT20 cell implantation. Volumes of individual tumors are shown, with horizontal line indicating the mean of each group at each time point (n=3, with an initial number of 5 mice per independent experiment, a number declining towards d35-42 because of gradual decease of mice); *, p<0.05.

(D) Gene expression in AMD3100-treated (20 days) and -untreated AtT20 xenograft tumors as determined by RT-qPCR. Bars show mean of fold AMD3100/control ± SEM (n=3 except for *Snai1* and *Snai2* where n=2); *, p<0.05.

(E) Effect of AMD3100 on AtT20 cell viability. Percentage of dying/dead AtT20 cells (as determined by trypan blue exclusion) after treatment with AMD3100 (*grey*) or vehicle (*black*). Bars show mean ± SEM (n=3); *, p<0.05.

(F) Effect of AMD3100 on AtT20 cell apoptosis. Percentage of $TUNEL^+$ cells after treatment with AMD3100 (*grey*) or vehicle (*black*). Bars show mean ± SEM (n=3); *, p<0.05.

(G) Effect of AMD3100 on AtT20 cell proliferation. Percentage of $Ki67^+$ AtT20 cells after treatment with AMD3100 (*grey*) or vehicle (*black*). Bars show mean ± SEM (n=3); *, p<0.05.

Fig. 5. Pituitary stem cells in the *Drd2*$^{-/-}$ pituitary tumor model

(A) Fold difference in absolute number of pSP cells in the anterior pituitary (AP) of homozygous *Drd2*$^{-/-}$ (n=5) and heterozygous *Drd2*$^{+/-}$ mice (n=2), relative to wildtype *Drd2*$^{+/+}$ mice (set as 1). *, p<0.05 *versus Drd2*$^{+/+}$ mice.

(B) Absolute number of $Sox2^+$ cells in the AP of homozygous *Drd2*$^{-/-}$, heterozygous *Drd2*$^{+/-}$ mice and wildtype *Drd2*$^{+/+}$ mice. Bars represent mean ± SEM (n=3), with indication of the nuclear-$Sox2^+$ cells

(*black segment*) and the cytoplasmic-Sox2$^+$ cells (*grey segment*). *, p<0.05 *versus* *Drd2*$^{+/+}$ mice (for total Sox2$^+$ cell number).

(C) Immunofluorescent staining of dissociated AP cells (cytospins) from wildtype *Drd2*$^{+/+}$ mice (*upper panel*) and homozygous *Drd2*$^{-/-}$ mice (*middle and lower panels*) for Sox2 (*red*) and Ki67 (*green*). Double Sox2$^+$/Ki67$^+$ cells are indicated (*arrows*). Nuclei are stained with DAPI. Representative examples are shown (female mice, 10-12 months of age). Scale bar: 50µm.

(D) Confocal images of pituitary vibratome sections of *Drd2*$^{-/-}$, *Drd2*$^{+/-}$ and wildtype *Drd2*$^{+/+}$ mice immunofluorescently stained for Sox2 (*red*) and prolactin (PRL, *green*). Representative examples are shown (female mice, 10-13 months of age). In all mouse phenotypes, Sox2$^+$ cells are found in the marginal cell layer along the cleft. In *Drd2*$^{-/-}$ pituitary Sox2$^+$ cells clustered in small groups are often observed within the PRL$^+$ tumor cell mass (*arrows*), but clusters of Sox2$^+$ cells are also found scattered in the anterior pituitary (AP) parenchyma of control *Drd2*$^{+/-}$ and *Drd2*$^{+/+}$ mice. Nuclei are stained with ToPro3. Scale bar: 50µm. *Insets* show a lower-magnification overview. IL, intermediate lobe.

SUPPLEMENTARY FIGURE LEGENDS

Fig. S1. Characterization of the side population (SP) in human pituitary adenomas

(A) Boxplot of SP proportions measured in pituitary adenoma samples immediately after surgical resection (*Fresh*; n=24) or after cryopreservation and thawing (*Frozen*; n=36). Minimum and maximum values (*whiskers*) and outliers (*dots*) are indicated.

(B) Forward scatter (FSC) and side scatter (SSC) of the adenoma SP cells (*blue*) compared to the MP cells (*orange*), both as gated in Fig. 1A.

(C) Principal Component analysis (PCA) of whole-genome expression data. A graphic is provided illustrating the distribution of the 9 micro-arrayed SPs (*grey*) and MPs (*black*) of pituitary adenomas along 2 principal components (as defined by Agilent's Feature Extraction Software).

(D) Hierarchical clustering of whole-genome expression data. *Upper panel:* schematic representation of gene expression levels in adenoma SP *versus* MP and resultant hierarchical clustering, using the probe sets (2760) identified as differentially expressed in the less stringent protocol (see Materials and Methods). *Lower panel*: schematic representation of gene expression levels in adenoma SP *versus* MP and resultant hierarchical clustering, using the probe sets (334) identified as differentially expressed in the more stringent approach (see Materials and Methods). Expression levels are indicated on a continuous color scale from downregulated (*green*) to upregulated (*red*) in the SP *versus* the MP. The SP samples are indicated by *grey* dots and the MP samples by *black* dots, as shown under each heat map.

Fig. S2. Genes differentially expressed between CD31$^-$/CD45$^-$ SP (pSP) and CD31$^-$/CD45$^-$ MP (pMP) from human pituitary adenomas

(A) Volcano plot (log_2-ratio *versus* minus log_{10} p-value) of whole-genome expression data from the pSP and pMP of human pituitary adenomas (n=5). Statistically upregulated genes (cut-off: fold-change ≥2 and uncorrected p<0.001; see Materials and Methods) are indicated in *red*, downregulated genes in *green*. It should be noted that many genes are scored altered by the fold-change criteria but not statistically significant because of the still relatively small number of samples analyzed.

(B) MA plot (average intensity *versus* log_2-ratio) of whole-genome expression data from the pSP and pMP of human pituitary adenomas (n=5). Statistically upregulated genes as determined in the Volcano plot are indicated in *red*, downregulated genes in *green*.

(C) Name of the microarray probes statistically upregulated (*left; red*) or downregulated (*right; green*) in the pSP *versus* pMP, as extracted from the Volcano plot.

(D) Immunohistochemical analysis of E-cadherin, vimentin, IL-6 and NOTCH2 in paraffin-embedded pituitary adenoma sections. Immunostaining for E-cadherin shows several immunonegative patches. Vimentin, IL-6 and NOTCH2 are found in some tumor cells (*arrows*),

either alone or in clusters. Vimentin is also present in pericapillar cells (*arrowheads*). Scale bar: 50 µm.

Fig. S3. Expression of stemness markers in spheres from human pituitary tumors

(A-B) Immunofluorescent analysis of spheres from human pituitary adenomas at day 7 of culture for SOX2 (*red*; A) or nestin (*green*; B). Nuclei are stained with ToPro3. Representative examples are shown (*left*: light-microscopic image; *right*: overlay).

(C) Immunofluorescent analysis of spheres from a human GH-A at day 8 of culture for SOX2 (*red*; A) and GH (*green*; B). Some sphere cells express the hormone produced by the original tumor (here, GH).

Scale bar: 50µm.

Fig. S4. Pituitary adenoma after transplantation under the kidney capsule

(A) H&E staining 6 months after transplantation of pituitary adenoma fragments under the kidney capsule of an immunodeficient SCID mouse, showing renal tissue (*pink*) and viable tumor tissue (*arrows*).

(B) Enlargement of the boxed area in A, showing the pituitary adenoma structure.

Scale bar: 50µm.

Fig. S5. Tumor growth from AtT20 and effect of TGFβ1

(A) AtT20 cells ($5x10^5$) were sc injected into SCID mice. Individual tumor volumes are shown, with horizontal line indicating the mean of each group at each time point (n=2, with an initial number of 4 mice per independent experiment).

(B) AtT20 SP (*black*) and MP (*grey*) were sc injected into SCID mice at the indicated number of cells (10 000, 5000 or 1000). Individual tumor volumes are shown, with horizontal line indicating the mean of each group at each time point (n=5 mice for 10 000 cells, n=4 mice for 5000 and

1000 cells; injected in 2 or 3 independent experiments); *, $p<0.05$. Some examples of dissected xenograft tumors are shown.

(C) AtT20 cells were pretreated with TGFβ1 or vehicle for 72 hr and then sc implanted in SCID mice. Individual tumor volumes are shown, with horizontal line indicating the mean of each group at each time point (n=3, with an initial number of 5 mice per independent experiment).

Fig. S6. Expression of the pituitary stem cell marker *Sox2* in pituitary tumor cell lines

(A) *Sox2* gene expression in the SP and MP from the AtT20 cell line and from the rat lactosomatotrope GH3 cell line as determined by RT-qPCR. Bars show mean fold SP/MP ± SEM (n=3); *, $p<0.05$.

(B) Dot plots of dual-wavelength FACS analysis of the GH3 cell line after incubation with Hoechst33342 alone (*left*), or together with verapamil (*right*). The SP (*black*) and MP (*white*) are gated and SP proportions are indicated. A representative example is shown.

Fig. S7. Pituitary stem cells in the *Drd2*$^{-/-}$ pituitary tumor model

(A) Transversal MRI pictures of the head of a female heterozygous *Drd2*$^{+/-}$ (*upper left panel*) and homozygous *Drd2*$^{-/-}$ (*lower left panel*) mouse at 8 months of age. The boxed region shows the pituitary, clearly bigger in the *Drd2*$^{-/-}$ mouse. Photographs of the pituitary *in situ* after euthanasia and removal of the brain in a heterozygous *Drd2*$^{+/-}$ (*upper row*) and homozygous *Drd2*$^{-/-}$ (*lower row*) mouse at 14 months of age. The pituitary of the *Drd2*$^{-/-}$ mouse is clearly bigger and contains large tumorous nodules. Scale bar: 1mm.

(B) Dot plots of dual-wavelength FACS analysis of *Drd2*$^{-/-}$ anterior pituitary (AP) after incubation with Hoechst33342 alone (*left*) or together with verapamil (*right*), and immunostained for CD31 and CD45. The SP (*black*) and MP (*white*) are gated and SP proportions are indicated. CD45^{+}, CD31^{+} and CD31^{-}/CD45^{-} cells within the SP are shown (*inset*). A representative example is given.

(C) Phase-contrast pictures of representative colonies formed after 4 days from *Drd2*$^{-/-}$ and *Drd2*$^{+/-}$ AP cells. Scale bar: 100µm.

(D) Additional pictures of Sox2 (*red*) and PRL (*green*) immunofluorescent staining in vibratome (A'-E') and paraffin-embedded (F' and G') sections of *Drd2*$^{-/-}$, *Drd2*$^{+/-}$ and wildtype *Drd2*$^{+/+}$ pituitaries (female mice, 10-13 months of age). In all mouse phenotypes, Sox2^{+} cells are found in the marginal cell layer along the cleft. In *Drd2*$^{-/-}$ pituitary, Sox2^{+} cells clustered in groups are often observed within the PRL^{+} tumor cell mass (B', *arrows*). Clusters are sometimes large in size (F' with blow-up in G'). Cytoplasmic-Sox2^{+} cells are more abundant in *Drd2*$^{-/-}$ than control pituitaries (*arrowheads*).

Nuclei were stained with ToPro3 (A'-E') or DAPI (F' and G'). Scale bar: 50µm. *Insets* show a lower-magnification overview. AP, anterior pituitary; IL, intermediate lobe.

Table 1. Summary of clinical and experimental data of the pituitary adenoma samples analyzed

Pituitary Adenoma (PA) sample number	Gender	Age at time of surgery (yr)	PA phenotype[a]	Size[b]	Fresh or cryopreserved	SP (% of total cells)	$CD31^+$ (% of SP)	$CD45^+$ (% of SP)	Micro-array	RT-qPCR	IHH
PA 01	M	62	NF-A	Macro	F	7.5	ND	ND			
PA 02	M	41	NF-A	Macro	F	1.5	ND	ND			
PA 03	M	46	GH-A	Macro	F	1.8	ND	ND	x		
PA 04	M	37	GH-A	Macro	F	1.4	ND	ND			
PA 05	F	28	GH-A	Macro	F	1.8	ND	ND			
PA 06	M	84	GH-A	Macro	F	1.4	ND	ND	x		
PA 07	F	76	GH-A	Macro	F	1.6	ND	ND	x		
PA 08	M	39	NF-A	Micro	F	2.0	ND	ND			
PA 09	F	54	NF-A	Macro	F	2.7	ND	ND			
PA 10	M	59	GH-A	Macro	C	2.3	ND	ND	x		
PA 11	F	59	GH-A	Macro	C	8.0	ND	ND			
PA 12	M	71	GH-A	Macro	C	1.8	ND	ND			
PA 13	F	44	ACTH-A	Micro	F	0.5	ND	ND			
PA 14	F	72	NF-A	Macro	C	1.2	ND	ND			
PA 15	M	79	NF-A	Macro	C	1.4	ND	ND			
PA 16	M	72	GH-A	Micro	C	0.7	ND	ND			
PA 17	M	35	NF-A	Macro	C	0.5	ND	ND	x		

PA 18	F	43	GH-A	Micro	C	1.2	ND	ND			
PA 19	F	57	NF-A	Macro	F	17.2	ND	ND	x		
PA 20	F	64	NF-A	Macro	F	1.5	ND	ND	x		
PA 21	F	48	ACTH-A	Micro	F	1.6	ND	ND			
PA 22	F	77	NF-A	Macro	C	3.3	ND	ND	x		Vim + IL-6 – Notch2 –
PA 23	F	29	NF-A	Macro	F	0.6	ND	ND	x		Vim + IL-6 + Notch2 +
PA 24	F	60	GH-A	Macro	C	1.6	18.2	ND			
PA 25	F	19	NF-A	Macro	F	0.8	89.9	ND			
PA 26	M	43	NF-A	Macro	C	4.8	93.8	ND			
PA 27	M	40	NF-A	Macro	C	1.8	87.2	ND			
PA 28	F	34	GH-A	Macro	F	0.8	38.9	ND			
PA 29	F	54	NF-A	Macro	C	1.5	93.8	ND			
PA 30	F	42	NF-A	Macro	C	1.3	70	7.9			
PA 31	M	76	NF-A	Macro	C	0.7	84	3.4			
PA 32	M	62	GH-A	Macro	F	1.3	81.6	4.8			
PA 33	M	80	NF-A	Macro	F	0.6	23.6	1.7	x	x	

PA 34	M	70	NF-A	Macro	F	1.3	24	27.3	x	x	Vim + IL-6 – Notch2 +
PA 35	M	40	NF-A	Macro	C	1.5	18.7	11.6	x	x	Vim – IL-6 – Notch2 –
PA 36	M	62	NF-A	Macro	C	0.6	71.6	17.8			
PA 37	F	50	GH-A	Micro	C	1.8	57.5	6.7			
PA 38	M	70	NF-A	Macro	C	0.6	60.9	3.9	x	x	Vim + IL-6 + Notch2 +
PA 39	F	39	PRL-A	Macro	C	1.2	43.3	33.5			
PA 40	M	63	NF-A	Macro	F	1.1	12.6	66.6	x	x	Vim + IL-6 + Notch2 +
PA 41	M	39	NF-A	Macro	F	0.9	22	3.9			
PA 42	F	30	NF-A	Macro	C	0.5	13	40.4			
PA 43	M	61	GH-A	Macro	C	6.8	95.2	1.3			
PA 44	M	49	NF-A	Macro	F	0.6	33	35		x	
PA 45	M	63	NF-A	Macro	F	2.4	60	4			
PA 46	F	27	GH-A	Macro	C	0.6	23	33.5		x	

PA 47	F	44	ACTH-A	Micro	C	1.5	5.8	37.3			
PA 48	F	39	NF-A	Macro	C	1.2	43.3	33.5			
PA 49	M	66	NF-A	Macro	C	0.4	80.7	2.4			
PA 50	F	28	PRL-A	Macro	C	1.4	75.5	4.6			
PA 51	F	77	GH-A	Macro	C	0.5	12.7	0.2			
PA 52	F	74	NF-A	Macro	C	1.7	81.5	5.5			
PA 53	F	62	GH-A	Macro	C	1.5	5.8	37.3			
PA 54	F	62	GH-A	Macro	C	1.9	29.7	23			
PA 55	M	62	NF-A	Macro	C	0.6	63.6	1.4			
PA 56	M	46	NF-A	Micro	C	1.6	75.9	1.1			
PA 57	M	45	GH-A	Macro	C	1.9	29.7	23			
PA 58	M	46	GH-A	Macro	C	1.9	29.7	23			
PA 59	M	52	NF-A	Macro	C	0.8	86	4.3			
PA 60	M	65	NF-A	Macro	C	0.5	48.4	1.1			

[a]NF-A, non-functioning adenoma; GH-A, somatotropinoma, ACTH-A, corticotropinoma; PRL-A, prolactinoma.

[b]Size: micro-adenoma: <1cm (micro); macro-adenoma: ≥1cm (macro).

ND, not determined; IHH, immunohistochemistry.

Table 2. Expression of a selection of genes in the total SP of human pituitary adenoma as concluded from microarray analysis

Gene[a]	Gene description	Expression in SP[b]
(Tumor) stemness		
ABCB1 (MDR/TAP)	ATP-binding cassette, sub-family B, member 1	
ABCG2 (BCRP1)	ATP-binding cassette, sub-family G (WHITE), member 2	
CD44	CD44 molecule (Indian bloud group)	
CXCR4	Chemokine (C-X-C motif) receptor 4	
KIT	v-kit Hardy-Zuckerman 4 feline sarcoma viral oncogene homolog	
KLF4	Kruppel-like factor 4 (gut)	
NES	Nestin	
Notch pathway (and related)		
DLL1	Delta-like 1 (Drosophila)	
DLL3	Delta-like 3 (Drosophila)	
DLL4	Delta-like 4 (Drosophila)	
HES1	Hairy and enhancer of split 1 (Drosophila)	
HES2	Hairy and enhancer of split 2 (Drosophila)	
HES5	Hairy and enhancer of split 5 (Drosophila)	
HEYL	Hairy/enhancer-of-split related with YRPW motif-like	
JAG1	Jagged 1	
NOTCH1	Notch 1	
NOTCH2	Notch 2	
NOTCH4	Notch 4	
TGFβ/BMP pathway (and related)		
BMP2	Bone morphogenetic protein 2	
BMP4	Bone morphogenetic protein 4	
BMP6	Bone morphogenetic protein 6	
MEN1	Multiple endocrine neoplasia 1	
SMAD2	SMAD family member 2	
SMAD3	SMAD family member 3	

SMAD4	SMAD family member 4	
TGFB1	Transforming growth factor, beta 1	
TGFB2	Transforming growth factor, beta 2	
TGFBR2	Transforming growth factor, beta receptor 2	
TGFBR3	Transforming growth factor, beta receptor 3	
WNT/β-catenin pathway (and related)		
APC	Adenomatous polyposis coli	
AXIN2	Axin 2	
CD44	CD44 molecule (Indian blood group)	
CDH1	E-cadherin (epithelial)	
CTNNB1	Catenin (cadherin-associated protein), beta 1, 88kDa	
DKK1	Dickkopf homolog 1 (Xenopus laevis)	
DKK2	Dickkopf homolog 2 (Xenopus laevis)	
FZD3	Frizzled family receptor 3	
FZD4	Frizzled family receptor 4	
FZD8	Frizzled family receptor 8	
LRP5	Low density lipoprotein receptor-related protein 5	
LEF1	Lymphoid enhancer binding factor 1	
MYC	v-myc myelocytomatosis viral oncogene homolog (avian)	
WNT9B	Wingless-type MMTV integration site 9B	
EMT		
Up in EMT		
CXCR4	Chemokine (C-X-C motif) receptor 4	
FN1	Fibronectin 1	
FOSL2	FOS-like antigen 2	
FOXC1	Forkhead box C1	
HOXB9	Homeobox B9	
KLF8	Kruppel-like factor 8	
MMP1	Matrix metallopeptidase 1 (interstitial collagenase)	
MMP2	Matrix metallopeptidase 2 (gelatinase A)	
SNAI1	Snail homolog 1 (Drosophila)	

TCF4	Transcription factor 4	
VIM	Vimentin	
ZEB1	Zinc finger E-box binding homeobox 1	
ZEB2	Zinc finger E-box binding homeobox 2	
Down in EMT		
CDH1	E-cadherin (epithelial)	
CLDN1	Claudin 1	
Angiogenesis/ endothelial		
CDH5	Cadherin 5, type 2 (vascular endothelium), VE-cadherin	
FLK1/KDR	Kinase insert domain receptor (a type III receptor tyrosine kinase)	
PECAM1 (CD31)	Platelet/endothelial cell adhesion molecule	
TEK/TIE2	Tyrosine kinase, endothelial	
TIE1	Tyrosine kinase with immunoglobulin-like and EGF-like domains 1	
VCAM1	Vascular cell adhesion molecule 1	
VWF	von Willebrand factor	
Immune/ hematopoietic		
CD45/PTPRC	Protein tyrosine phosphatase, receptor type C	

[a]Selection of genes as analyzed by microarray; genes are listed alphabetically per group.

[b]Expression level of the gene in the total adenoma SP: (▨) when >1.5-fold upregulated in the SP *versus* the MP in at least 2/3rd of the adenoma samples analyzed (6 or more out of the 9); (▭) when >1.5-fold upregulated in the SP *versus* the MP in 5 out of the 9 adenoma samples; (▥) when >1.5-fold downregulated in the SP *versus* the MP of at least 6 out of the 9 adenoma samples analyzed. Indicated as (▭) when <1.5-fold difference *versus* MP.

Table 3. Expression of a selection of genes in the pSP of human pituitary adenoma as concluded from microarray analysis

Gene[a]	Gene description	Expression in pSP[b]
(Tumor) stemness		
ABCG2 (BCRP1)	ATP-binding cassette, sub-family G (WHITE), member 2	
CD34	CD34 molecule	
CD44	CD44 molecule	
CXCR4	Chemokine (C-X-C motif) receptor 4	
KIT	v-kit Hardy-Zuckerman 4 feline sarcoma viral oncogene homolog	
LIFR	Leukemia inhibitory factor receptor	
*NES**	Nestin	
Notch pathway (and related)		
*DLK1**	Delta-like 1 homolog	
*DLL1**	Delta-like 1	
*DLL3**	Delta-like 3	
*DLL4**	Delta-like 4	
*HES1**	Hairy and enhancer of split1	
*HEY2**	Hairy/enhancer-of-split related with YRPW motif 2	
*JAG1**	Jagged1	
*JAG2**	Jagged 2	
*NOTCH1**	Notch gene homolog 1	
NOTCH2	Notch gene homolog 2	
*NOTCH4**	Notch gene homolog 4	
TGFβ/BMP pathway (and related)		
BMP2	Bone morphogenetic protein 2	
BMPR2	Bone morphogenetic protein receptor 2	
TGFB2	Transforming growth factor, beta 2	
*TGFB1**	Transforming growth factor, beta 1	
TGFBI	Transcription factor, beta-induced	

TGFBR2	Transforming growth factor, beta receptor II	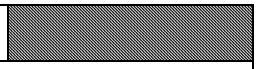
WNT/β-catenin pathway (and related)		
*DKK1**	Dickkopf homolog 1	
*DKK2**	Dickkopf homolog 2	
DKK3	Dickkopf homolog 3	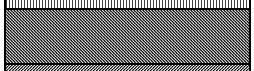
DKK4	Dickkopf homolog 4	
*FZD1**	Frizzled 1 homolog	
FZD10	Frizzled 10 homolog	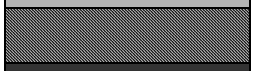
*TCF3**	Transcription factor 3	
TCF7L1	Transcription factor 7-like 1	
TCF7L2	Transcription factor 7-like 2	
*WNT5a**	Wingless-related MMTV integration site 5A	
EMT		
CXCR4	Chemokine (C-X-C motif) receptor 4	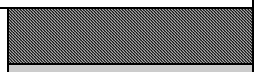
FN1	Fibronectin	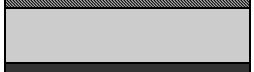
*SNAI1**	SNAIL homolog 1	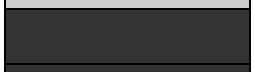
*SNAI2 (SLUG)**	SNAIL homolog 2	
VIM	Vimentin	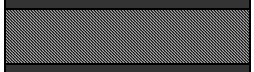
*ZEB1**	Zinc finger E-box binding homeobox 1	
ZEB2	Zinc finger E-box binding homeobox 2	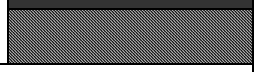
Angiogenesis/ endothelial		
VCAM1	Vascular cell adhesion molecule 1	
VWF	von Willebrand factor	

[a]Selection of genes as analyzed by microarray; genes are listed alphabetically per group

[b]Expression level of the gene in the adenoma $CD31^-/CD45^-$ SP (pSP): (▨) when >1.5-fold upregulated in pSP *versus* pMP in all 5 of the adenoma samples; (▭) in 4 out of the 5 tumors; (■) in 3 out of the 5 tumors; (▥) in 2 out of the 5 tumors; (▨) when >1.5-fold downregulated in at least 3 of the 5 tumors. Indicated as (▭) when <1.5-fold difference *versus* MP.

* means >1.5-fold upregulation but p>0.05.

Fig. 1

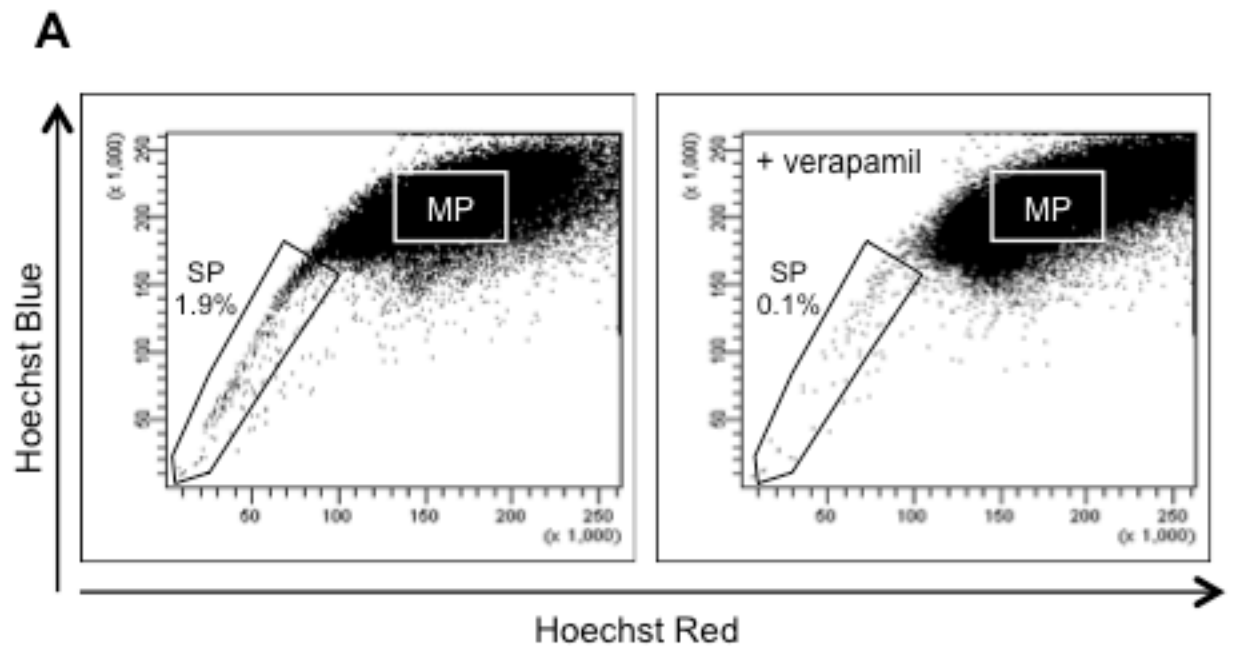
A
Hoechst Blue
Hoechst Red
MP
SP
1.9%
+ verapamil
SP
0.1%
(x 1,000)

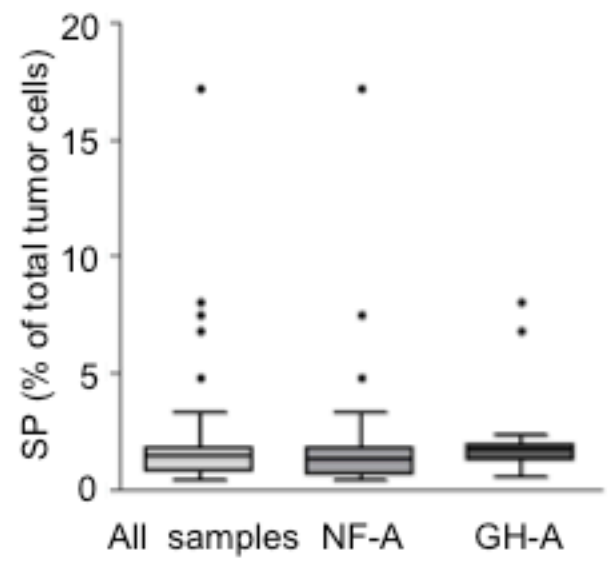
B
SP (% of total tumor cells)
20
15
10
5
0
All samples
NF-A
GH-A

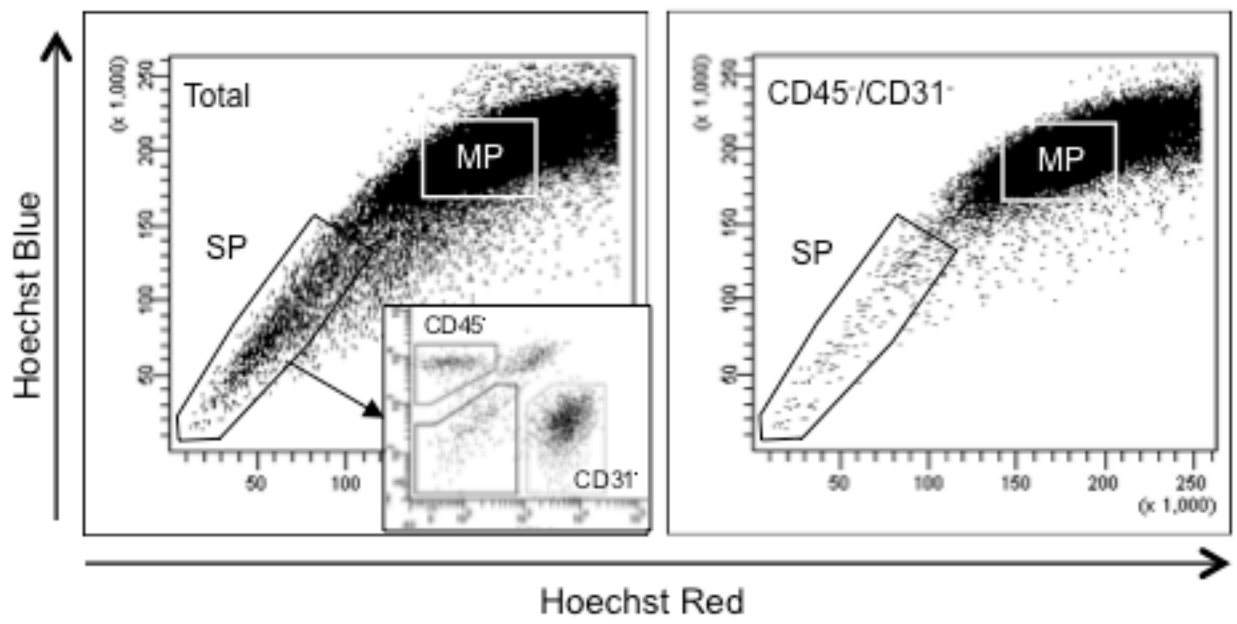
C
Hoechst Blue
Hoechst Red
Total
MP
SP
CD45-
CD31-
CD45-/CD31-

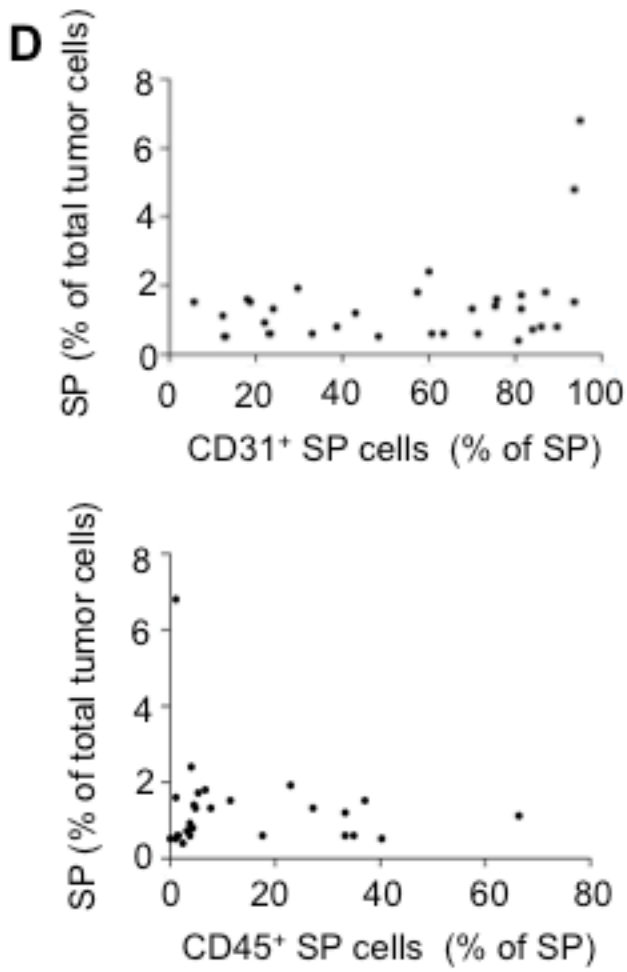
D
SP (% of total tumor cells)
CD31+ SP cells (% of SP)
CD45+ SP cells (% of SP)

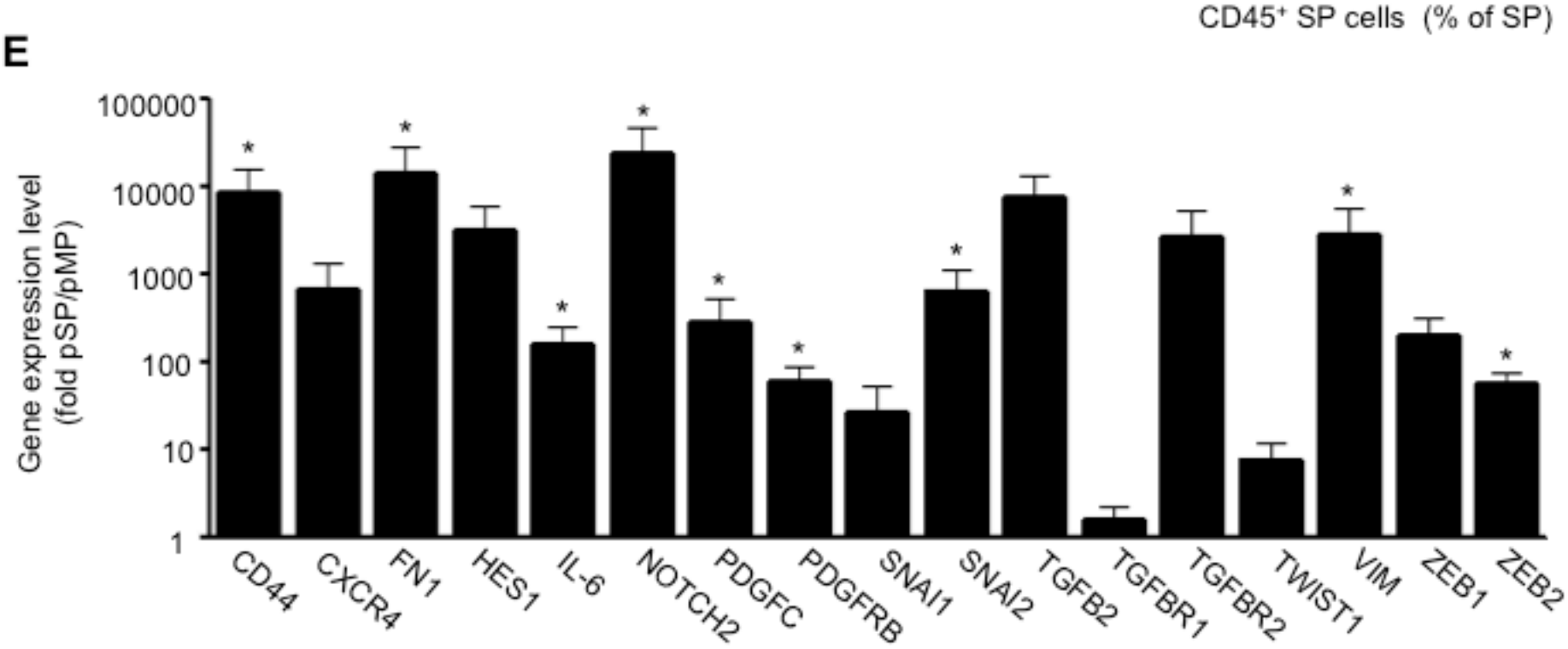
E
Gene expression level
(fold pSP/pMP)
100000
10000
1000
100
10
1
CD44
CXCR4
FN1
HES1
IL-6
NOTCH2
PDGFC
PDGFRB
SNAI1
SNAI2
TGFB2
TGFBR1
TGFBR2
TWIST1
VIM
ZEB1
ZEB2

Fig. 2

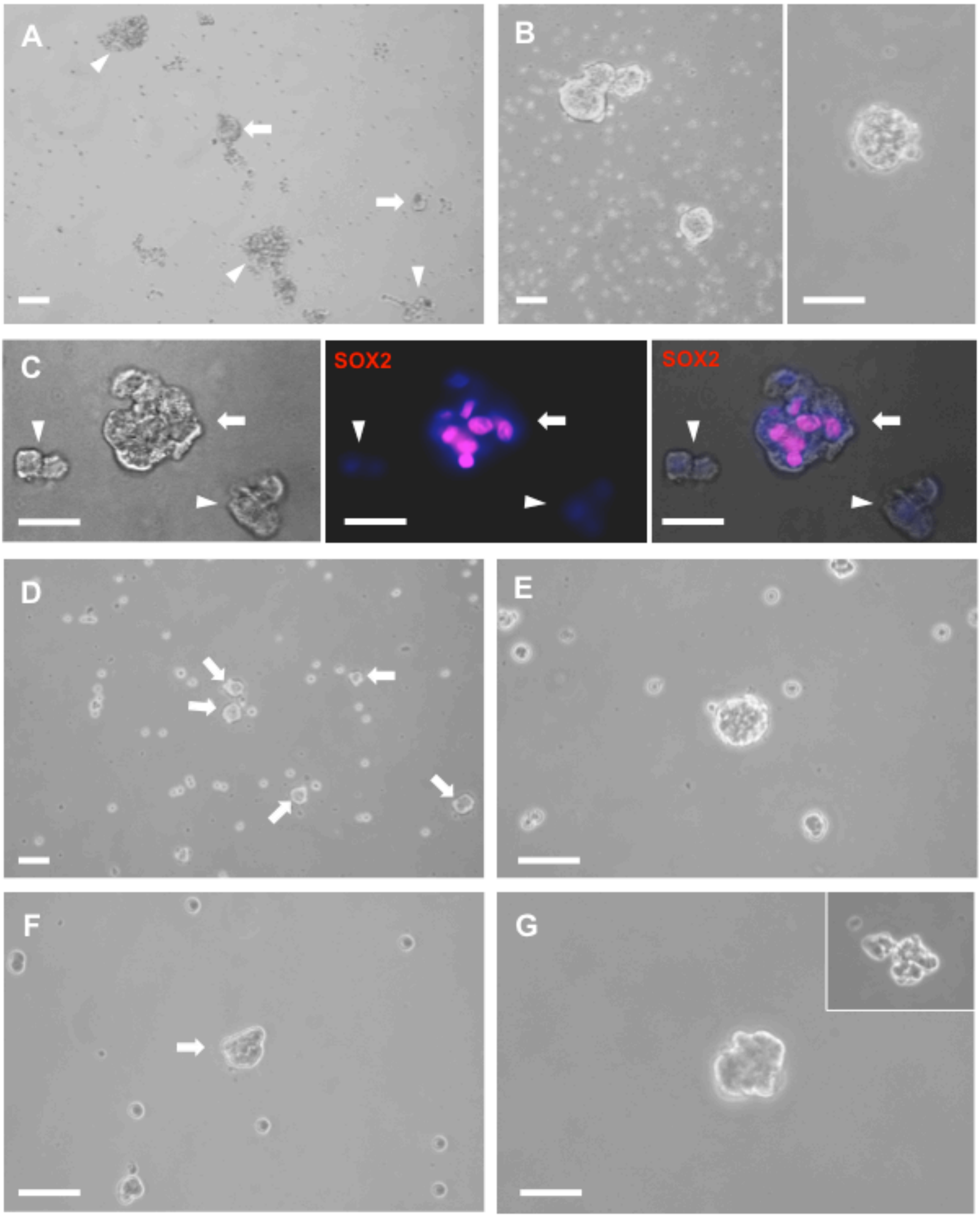

Fig. 3

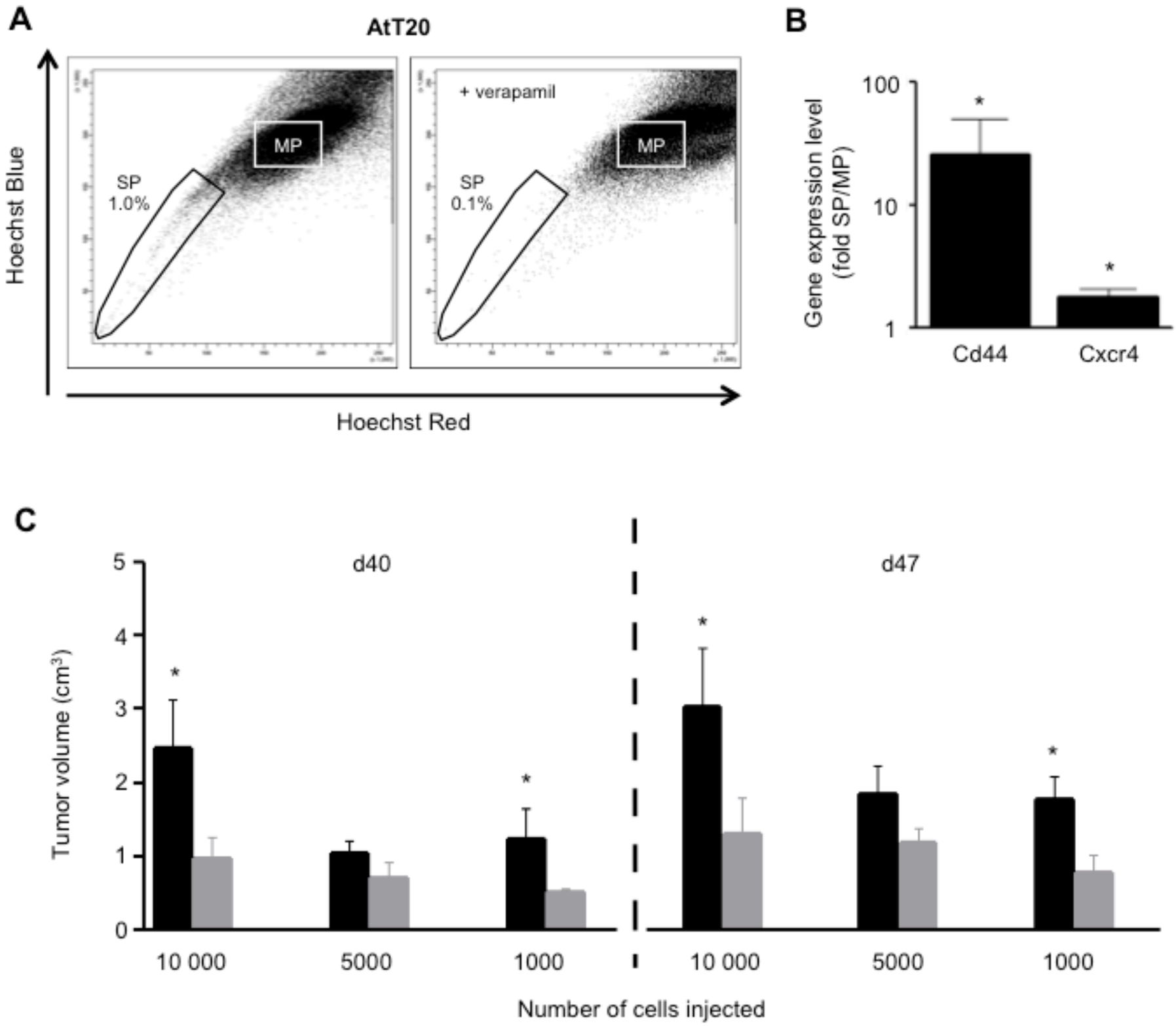
A
AtT20
Hoechst Blue
Hoechst Red
MP
SP
1.0%
+ verapamil
MP
SP
0.1%
B
Gene expression level
(fold SP/MP)
100
10
1
*
*
Cd44
Cxcr4
C
d40
d47
Tumor volume (cm³)
5
4
3
2
1
0
*
*
*
*
10 000
5000
1000
10 000
5000
1000
Number of cells injected

Fig. 4

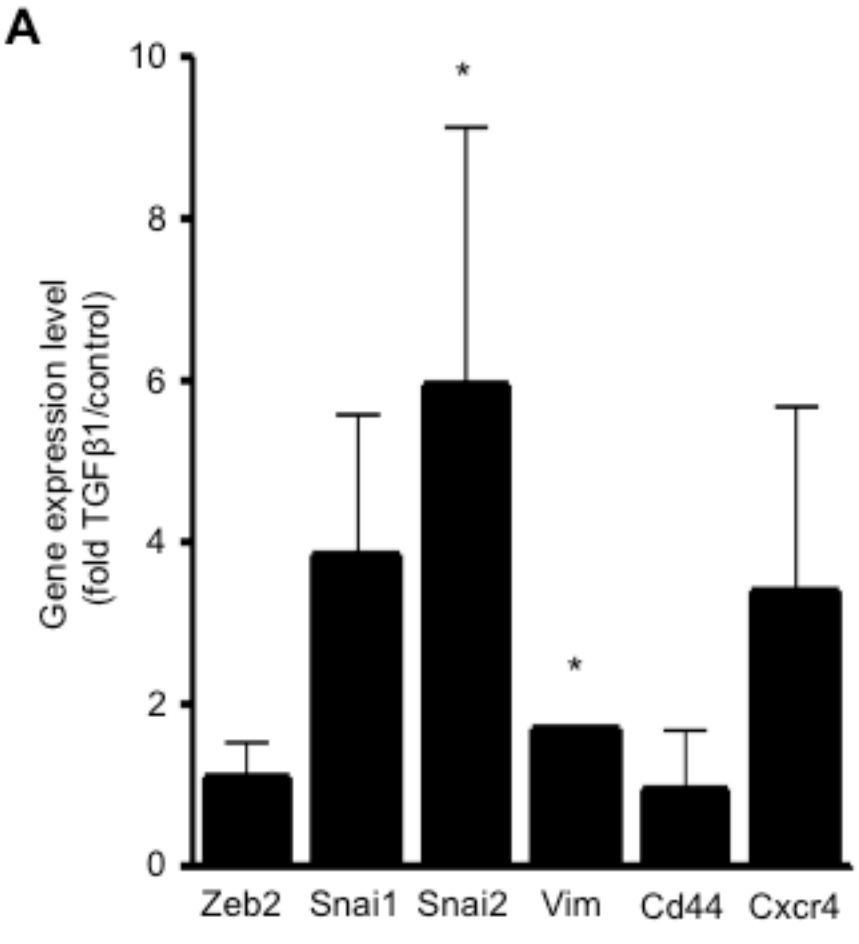
A
Gene expression level (fold TGFβ1/control)
10
8
6
4
2
0
*
*
Zeb2
Snai1
Snai2
Vim
Cd44
Cxcr4

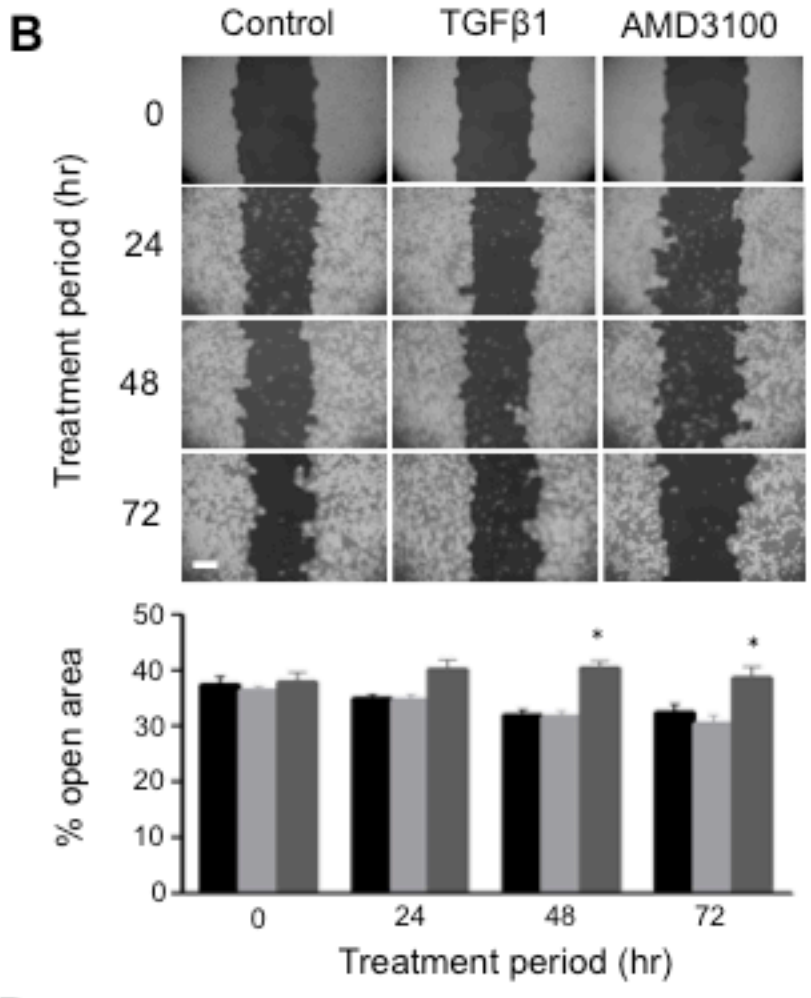
B
Control
TGFβ1
AMD3100
Treatment period (hr)
0
24
48
72
% open area
50
40
30
20
10
0
*
*
0
24
48
72
Treatment period (hr)

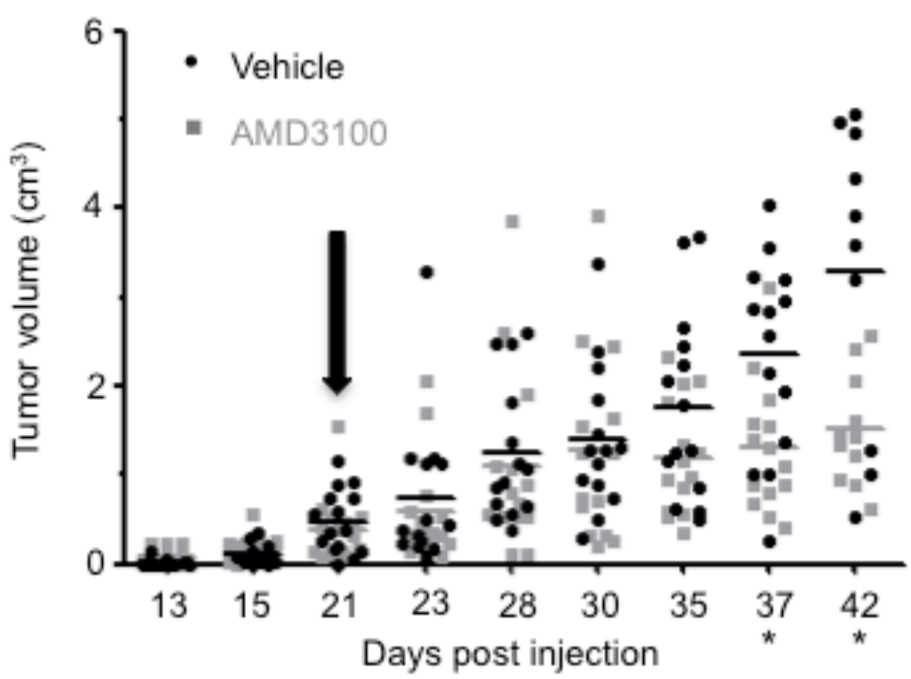
C
Vehicle
AMD3100
Tumor volume (cm³)
6
4
2
0
13
15
21
23
28
30
35
37
42
*
*
Days post injection

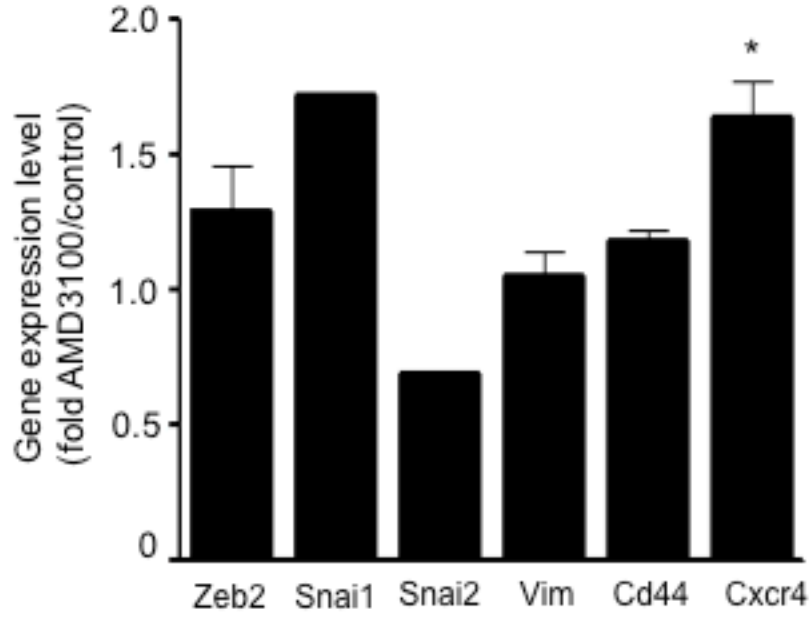
D
Gene expression level (fold AMD3100/control)
2.0
1.5
1.0
0.5
0
*
Zeb2
Snai1
Snai2
Vim
Cd44
Cxcr4

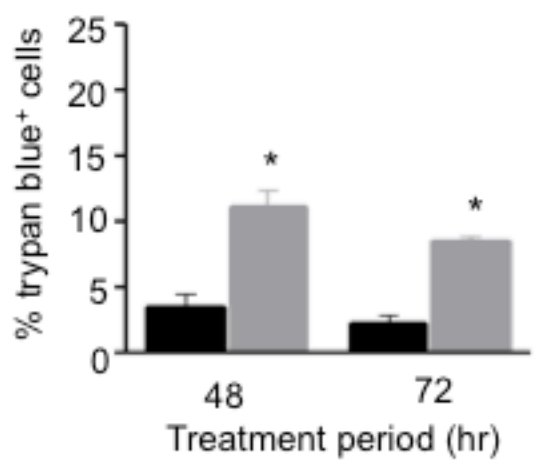
E
% trypan blue⁺ cells
25
20
15
10
5
0
*
*
48
72
Treatment period (hr)

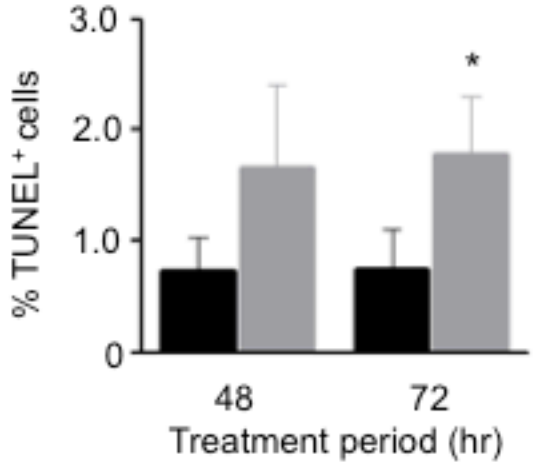
F
% TUNEL⁺ cells
3.0
2.0
1.0
0
*
48
72
Treatment period (hr)

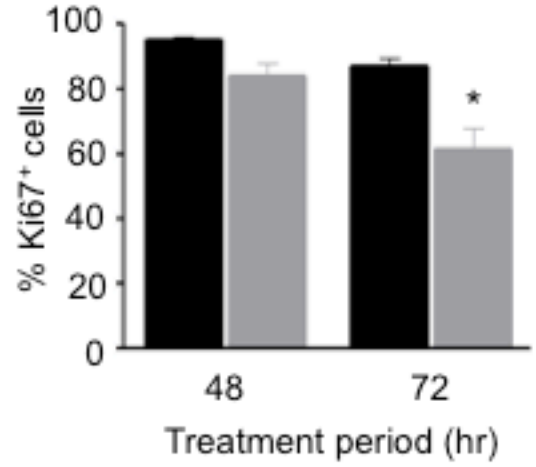
G
% Ki67⁺ cells
100
80
60
40
20
0
*
48
72
Treatment period (hr)

Fig. 5

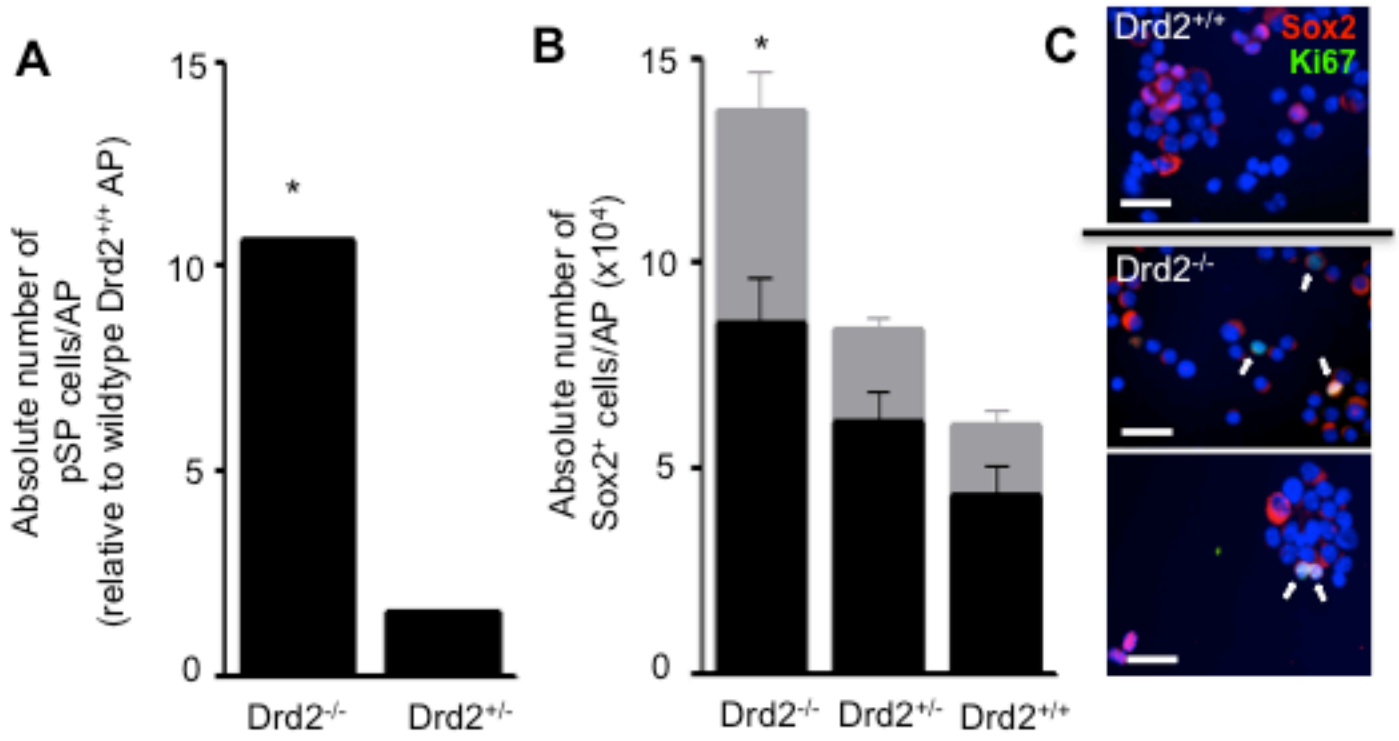
A
Absolute number of pSP cells/AP (relative to wildtype Drd2+/+ AP)
15
10
5
0
*
Drd2-/-
Drd2+/-
B
Absolute number of Sox2+ cells/AP (x10^4)
15
10
5
0
*
Drd2-/-
Drd2+/-
Drd2+/+
C
Drd2+/+
Sox2
Ki67
Drd2-/-

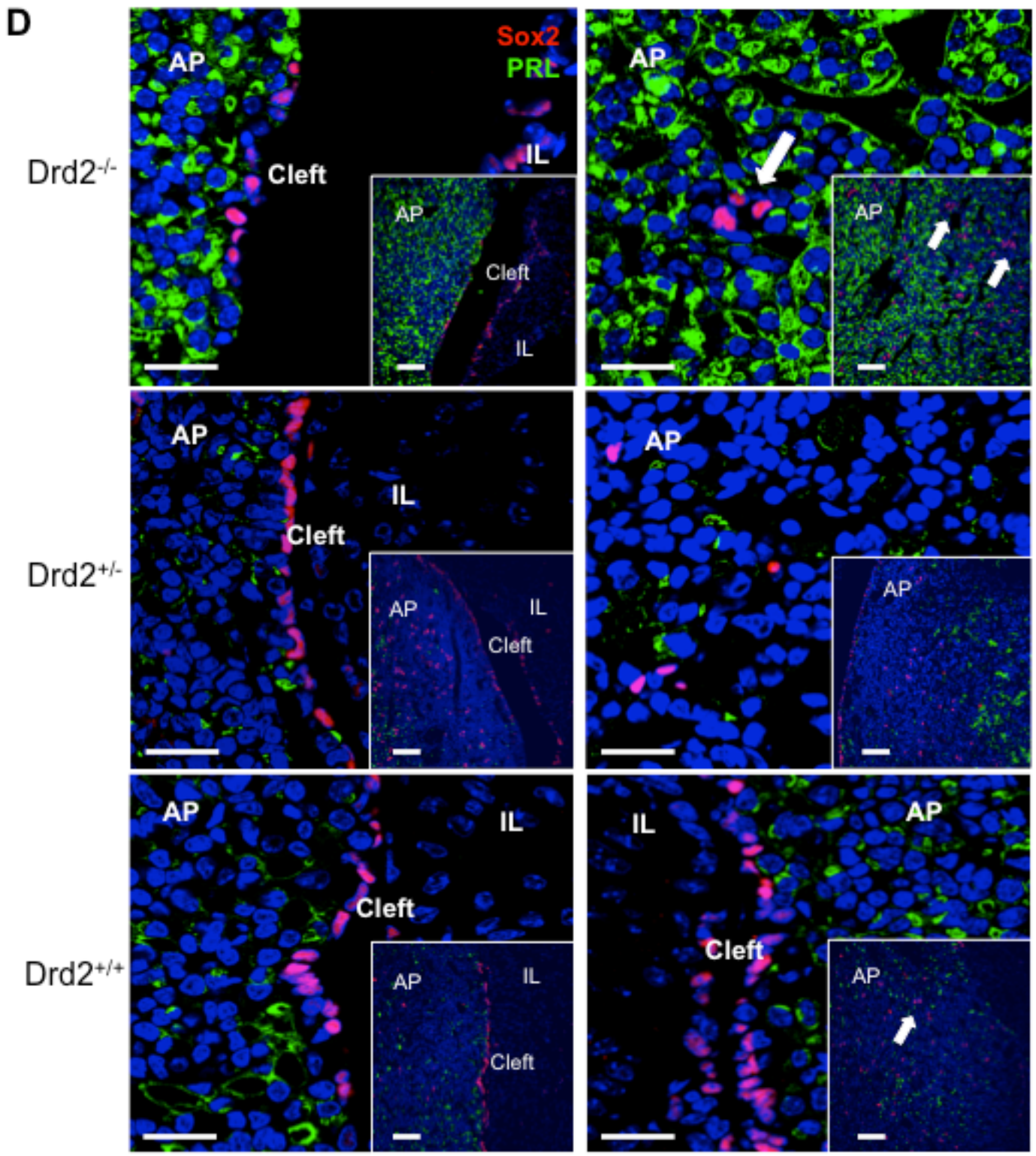
D
Drd2-/-
Drd2+/-
Drd2+/+
AP
Cleft
IL
Sox2
PRL